Nanomembrane-assembled nanophotonics and optoelectronics: from materials to applications

IOP Publishing Journal of Physics: Condensed Matter
J. Phys.: Condens. Matter **35** (2023) 093001 (19pp) https://doi.org/10.1088/1361-648X/acabf3

Topical Review

Nanomembrane-assembled nanophotonics and optoelectronics: from materials to applications

Jiayuan Huang[1], Gaoshan Huang[1], Zhe Zhao[1], Chao Wang[1], Jizhai Cui[1], Enming Song[2] and Yongfeng Mei[1,*]

[1] Department of Materials Science, International Institute of Intelligent Nanorobots and Nanosystems, Institute of Optoelectronics, Yiwu Research Institute, State Key Laboratory of ASIC and Systems, Fudan University, Shanghai 200433, People's Republic of China
[2] Shanghai Frontiers Science Research Base of Intelligent Optoelectronics and Perception, Institute of Optoelectronics, Fudan University, Shanghai 200433, People's Republic of China

E-mail: yfm@fudan.edu.cn

Received 6 June 2022, revised 11 October 2022
Accepted for publication 15 December 2022
Published 23 December 2022

Abstract

Nanophotonics and optoelectronics are the keys to the information transmission technology field. The performance of the devices crucially depends on the light–matter interaction, and it is found that three-dimensional (3D) structures may be associated with strong light field regulation for advantageous application. Recently, 3D assembly of flexible nanomembranes has attracted increasing attention in optical field, and novel optoelectronic device applications have been demonstrated with fantastic 3D design. In this review, we first introduce the fabrication of various materials in the form of nanomembranes. On the basis of the deformability of nanomembranes, 3D structures can be built by patterning and release steps. Specifically, assembly methods to build 3D nanomembrane are summarized as rolling, folding, buckling and pick-place methods. Incorporating functional materials and constructing fine structures are two important development directions in 3D nanophotonics and optoelectronics, and we settle previous researches on these two aspects. The extraordinary performance and applicability of 3D devices show the potential of nanomembrane assembly for future optoelectronic applications in multiple areas.

Keywords: nanomembrane, assembly, nanophotonics, optoelectronics

(Some figures may appear in colour only in the online journal)

1. Introduction

In recent years, nanophotonics and optoelectronics have become a crucial development direction in the information technology field. Optoelectronic information technology involving important fields such as light detection, laser and sensing is the dominant technology of the future information industry. The development of nanophotonics/optoelectronics has brought important technological breakthroughs to the scientific field, providing the possibility to build fully functional optoelectronic devices at the nanoscale. To obtain wave information of ultraviolet, visible, infrared and even terahertz bands emitted by targets, optoelectronic devices help convert optical signals into electrical signals [1–3]. It can be used to obtain electromagnetic signals so as to accurately identify and

* Author to whom any correspondence should be addressed.

analyze targets in various environments, thus greatly expanding the observation ability of human eyes.

As the key to optoelectronic conversion, the performance of optoelectronic devices will directly affect the entire photoelectric information system [4]. It is of great significance to improve the optoelectronic performance (such as sensitivity, specific detection rate, sub-threshold swing, photoelectric conversion efficiency, etc) of devices. Most importantly, the performance of optoelectronic devices depends on the absorption of light by the material, as well as the light–matter interaction. At present, related researches focus on two aspects: the addition of functional materials and the design of optical structures. In terms of new functional materials, novel materials, low-dimensional materials and a variety of two-dimensional (2D) materials have been used to prepare photodetectors [5, 6]. On the other hand, several optical structures are introduced to improve light absorption. Optical microcavity [7], metal grating [8], surface plasmon structure [9], and other structures have been successfully used for performance improvement. In addition, although most of the functional layers of photodetectors exist in a planar form, recent studies show that devices of three-dimensional (3D) structures present better light field regulation ability and application advantages [10–12].

The common fabrication techniques of micro/nano three-dimensional (3D) structures mainly include 3D printing, 3D lithography, 3D stacking, and so on. However, 3D printing and 3D lithography are relatively limited in materials, which confine their applications in the semiconductor field and it is generally difficult to fabricate 3D structures with large depth [13, 14]. 3D stacking is greatly limited in structure, and the requirements of 3D etching and deposition also restrict its further development [15]. Therefore, 3D assembly of nanomembranes has attracted increasing attention recently due to its low cost, high sensitivity and integratability [16–19]. The applications of lithographic patterning techniques on nanomembranes enable the fabrication of 3D devices compatible with backplane architectures such as the complementary metal-oxide-semiconductor (CMOS) [20, 21]. While for the material aspect, semiconductor materials of IV and III–V groups obtain high quality responses to light owing to their intrinsic properties [22–25]. 2D layered materials such as graphene and MoS_2 are also widely used due to their atomic thickness, flexibility, enhanced light–matter interactions, and the ability to form heterostructures bonded by van der Waals forces [26, 27]. 3D assembly techniques based on nanomembranes made from above materials, including rolling, folding, buckling and pick-place methods, have already been used to prepare novel devices for nanophotonics and optoelectronics. In order to realize the large-scale fabrication of practical 3D devices, plenty of researches have focused on the structure-function relationship of 3D structure, the certainty and controllability of fabrication on device performance, as well as the development of the on-chip integration technology [28–31].

In this review, we first introduce nanomembranes of versatile materials including semiconductors, metals, 2D materials that can be applied in nanophotonics and optoelectronics. The construction of 3D devices is then described in terms of fabrication, patterning, release and most importantly assembly. Due to the unprecedented physical properties and applicable functions brought by nanomembrane assembly and the addition of different functional materials, 3D micro/nano devices can be expected to have great potential for future optoelectronic applications. The main content of this review is schematically shown in figure 1.

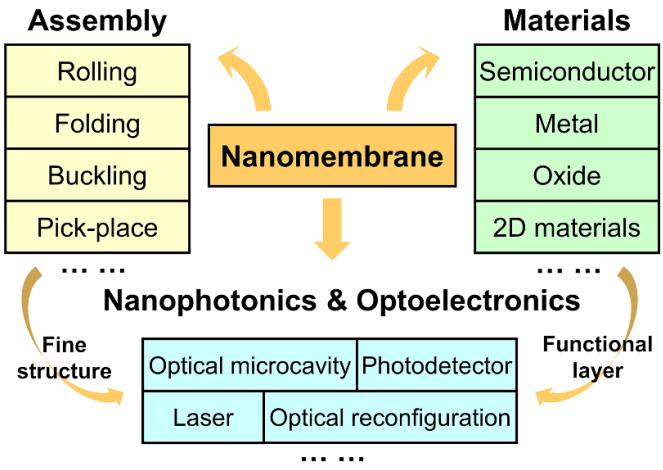

Figure 1. Schematic illustration of the framework of this review.

2. Brief to materials and processing of optoelectronic nanomembranes

2.1. Basic concept of nanomembrane

Traditional solid film usually refers to a dimension of the scale of the material that is 1 ∼ 2 orders of magnitude smaller than the sizes of the other two [32]. While the concept of nanomembrane was first developed from nanoscience and defined differently by various literature. Generally, nanomembrane can be described as a film of which the thickness is limited by nanoscale between ∼1 and ∼100 nm [33], and is usually isolated from the environment on both sides (e.g. by air, vacuum, or other different materials). The other definition refers to the characteristics about freestanding and self-support of nanomembranes [34]. As mentioned, nanomembrane is the nearest ideal 2D structure, which can be taken as nano-objects for its ultra-thin thickness, as well as macroscopic objects for its large lateral area. Nanomembrane mentioned above has no limitation on the composition. For the dimensional confinement, nanomembrane shows its high specific surface area and feature size between atomic and macro scale, which causes special properties different from the macroscopic object of the same material [35, 36].

2.2. Compositions of optoelectronic nanomembranes

To meet the demand for miniatured optoelectronic and nano-optical devices, various materials are reported to be applied in nanomembranes, which certainly support diverse physical properties of nanomembranes and corresponding devices with broad application potentials.

Due to the special properties of semiconductor in light response, semiconductor nanomembranes are widely used in the application of optoelectronics. As the most typical semiconductor material, Si nanomembrane can be advantageously used in optoelectronics based on the suitable band gap that can achieve high quality light response in visible region [22]. Different from bulk materials, the small thickness of Si nanomembrane brings special optoelectrical properties [37]. Several modifications to tune the optical properties of Si nanomembrane are reported. For example, ultrathin Si nanomembranes with treated rough surfaces were found to demonstrate a giant persistent photoconductivity effect [38]. Since the rough surface inhibits the carrier transmission, the dark current of the Si nanomembrane transistor was very small under the positive bias voltage [38]. However, the current was significantly increased while illuminated, and the highly charged state of light activation can last for a long time after removing light sources, leading to persistent photoconductivity. In addition, surface roughing can improve the thermoelectric properties of nanomembrane assembled by Si nanowires (NWs) [39]. Most importantly, the nanoscale thickness of single-crystalline Si nanomembrane overcomes the fracture and performance degradation, bringing high mechanical flexibility and transferability [40]. After being released from the original substrate, Si nanomembranes can be transferred to a variety of substrates to form heterogeneous integrations between various material combinations to achieve multiple functions and plentiful devices [41]. For market requests, the Si nanomembrane is also popular for its technical compatibility with the mature CMOS fabrication technology.

Limited by the inherent band gap, the response spectral range of Si nanomembrane is mainly around visible region. In order to develop a light response in infrared region, materials with narrow band gap such as III–V group materials and Ge are suggested to possibly build heterogenous integration with Si substrate [42, 43]. Because of the lattice constant mismatch between III–V compounds/Ge and Si substrate, tensile strain in these material layers also decreases the bandgap energy to extend the light response range by lowering the conduction-band edge and raising the valence-band maximum [44, 45]. In addition, quantum wells (QWs)/ quantum dots (QDs) are also embedded in standard III–V semiconductor nanomembranes to enhance the light absorption as gain media, which can take advantage in photodetection and lasing [11, 46, 47].

However, these semiconductor nanomembranes cannot fully satisfy the upcoming market for bendable and wearable optoelectronic devices, which require even more flexible materials [48]. Therefore, novel photoelectronic devices are now also developed on the basis of 2D layered materials [49]. At present, through the use of appropriate 2D layered materials with atomic thickness, flexibility and strong light–matter interaction enhancement can be achieved in heterostructures linked by van der Waals forces [50, 51]. Specifically, MoS_2 is attractive for its excellent semiconducting properties at atomic thicknesses [52, 53]. Owing to a direct band gap of 1.9 eV in monolayer MoS_2, this material is well suitable for applications in optoelectronics [54]. Graphene nanomembrane, another good candidate, exhibits superlative mechanical, thermal, biocompatible and charge transport properties, which are unavailable for bulk graphite. Considering the good performance when being integrated with conventional devices, graphene nanomembranes can provide more device opportunities for application in nanophotonics [8] and optoelectronics [55].

Pure metal nanomembranes support special electron behavior such as surface plasmon polaritons can be also applied as a common visible light gain media [56]. Metal materials including gold, silver, aluminum and chromium can support plasmonic response at their interface with dielectric medium [57]. Considering the biological compatibility of gold, on-chip biological sensors can be designed based on the gold nanomembranes due to the corresponding light–matter enhancement effect [58]. Further, gold NWs can also be arranged into nanomembrane structures with high strength and optical transparency [59].

It is worth noting that multilayered nanomembrane consisting of several materials is also widely utilized to recover the defect for single composition materials. With the development direction of miniaturized devices, on-chip integration is another important trend except for optimizing optoelectronic properties. Researchers will no longer unilaterally pursue the reduction of feature size but develop comprehensive innovations such as the addition of functional layers to improve the performance and integration of optoelectronic devices [60]. Heterogeneous integration technology is an important technical approach, which can extend the preparation of optoelectronic devices composed of multilayer nanomembrane of functional materials along the vertical direction, and effectively reduce the power consumption and device/chip footprint [61].

2.3. Processing and assembly of optoelectronic nanomembrane

The nanomembrane processing, including the fabrication, patterning, release and 3D assembly, can be briefly described in figure 2 and will be detailed in the following parts.

2.3.1. Fabrication of nanomembrane. As the most important feature of nanomembranes, thickness can be determined by the growth process and mechanism during the formation. Generally, the fabrication methods can be classified into top–down approach and bottom–up one (figure 2(a)).

Thinning bulk materials is a common method of top–down fabrication for nanomembranes. Mechanical exfoliation was first used to separate monolayers from graphite [62] to obtain fabrication of graphene nanomembrane, and then applied to other layered materials. In order to improve productivity, chemical exfoliation [63] and sonication exfoliation [64] are also used. In addition, Si nanomembranes can be obtained from silicon-on-insulator (SOI) wafer by etching the oxide layer between the top Si layer and bottom Si substrate. The top single-crystalline nanomembrane released from SOI wafer was found to possess unique optoelectronic properties [65].

For bottom–up fabrication, vapor phase deposition is commonly used. The approach includes physical vapor deposition

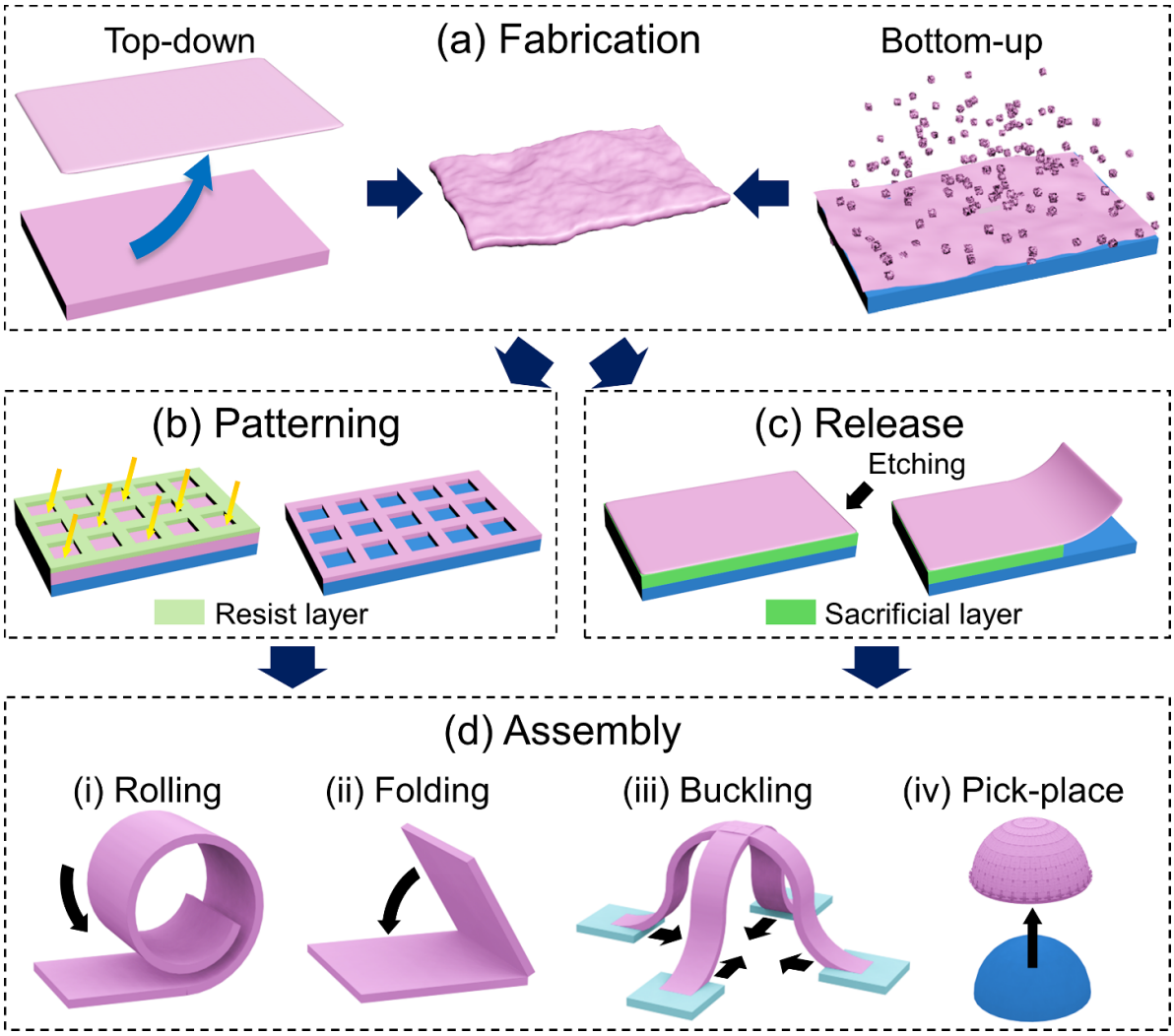

Figure 2. Typical processing steps of nanomembranes, including (a) fabrication, (b) patterning, (c) release and (d) 3D assembly. (a) The fabrication processes of nanomembranes are commonly divided to top–down and bottom–up approaches. (b) The patterning of nanomembrane almost depend on the lithography techniques. (c) Release of nanomembrane relies on selective removal of sacrificial layer. (d) The most common 3D assembly methods include (i) rolling, (ii) folding, (iii) buckling and (iv) pick-place approaches.

(PVD) [66], chemical vapor deposition (CVD) [67], molecular beam epitaxy (MBE) [68], atomic layer deposition (ALD) [69], etc. Evaporation and sputtering are the most widely used PVD process, by which the composition of nanomembrane is mainly determined by targets. Due to the less limitation of target materials, various nanomembranes of semiconductor [70] and metal [47] materials deposited by PVD can be obtained. CVD is also widely used for coating layers and nanomembrane of various materials because of their affordable cost and controllable precursor [71, 72]. For example, the formation of SiN_x nanomembrane can be realized by the addition proportion of silane and nitrogen [73–75] and the vertical strain contrast in the nanomembrane is also introducible during CVD process. MBE is utilized to effectively deposit single crystal materials at low temperatures in a high vacuum or ultrahigh vacuum. The low deposit rate of MBE processes can bring high quality of the nanomembrane ideal for nanoscale photonic and optoelectronic devices [76]. ALD is a useful method of forming nanomembranes by alternately passing a vapor precursor pulse into a reactor, in which chemically adsorption and reaction happen on the deposited matrix [77, 78]. ALD demonstrates superiority in accurate control of the thickness of nanomembrane [79]. Due to the excellent conformality, ALD processes can also be used to increase the thickness of oxide nanomembrane in order to control the optical properties [69].

Moreover, other deposition methods such as sol–gel method [80] and hydrothermal/solvothermal synthesis [81] can be applied in the fabrication of nanomembranes as well. For organic materials, nanomembranes were fabricated by normal spin-coating [82] and layer-by-layer assembly process [83].

Except for common synthesis methods, self-assembly of nanoparticles (NPs), NWs and other nanostructured building blocks, instead of molecules and atoms, for fabrication of nanomembranes are also important synthesis approaches in previous literature [84–87]. The self-assembly can be realized by the Langmiur–Blodgett technique at the liquid–air interface

[88] or the evaporation of solvent at the liquid–liquid interface [89, 90]. Recent researches mostly focus on the assembly of NPs at the liquid–liquid interface [91–93]. For example, by mixing droplet of hydrophilic NPs solution into hydrophobic solvent [94] or adding droplet of organic NPs into water [95], NPs can be confined to the interface by the free energy reduction comparable to thermal energy [91]. Specifically, Li *et al* [94] dispersed $CuGaO_2$ NPs to water phase, and the NPs were trapped at a water-hexane interface to build a nanomembrane; Cai *et al* [89] added octadecene to chloroform solution of Fe_3O_4 NPs, heated and agitated the mixture, and assembled nanomembrane was finally produced by evaporation of the solvent. By tuning the concentration of solvent [89] or the contact angle of the interface [96], the self-assembly of nanomembrane can be intentionally designed and controlled. Similarly, self-assembly of NWs is also investigated [59]. Gong *et al* [97] reported that mesh nanomembrane can be prepared by self-assembly via casting NWs droplets onto the air-water interface. The organization of these nanoscale building blocks can be considered as an important alternative way for nanomembrane fabrication.

2.3.2. Patterning and release of nanomembrane. For further application in nanophotonics and optoelectronics, fabricated nanomembranes need more treatments to be shaped/constructed into various geometries. Patterning (figure 2(b)) is a necessary step for following construction process, especially for sophisticated structures. To broaden the application scenario on different substrates, separation of nanomembrane and original substrate, i.e. release process is also important.

One of the easiest patterning methods is mechanical scratching with sandpaper, which can bring some strips or rectangle patterns for a quick test but with very low accuracy [98]. Lithography is widely used in microelectronics industries, including photolithography and E-beam lithography. For a given nanomembrane to be patterned, a resist layer is usually coated on it at the beginning of the lithography process. The pattern can be formed on the resist layer through an exposure-development procedure [99]. Photolithography which uses ultraviolet radiation can be utilized to produce high parallel structures on one substrate, for the reason that lithography patterns on the photomask can be simultaneously duplicated. The parallel pattern with microscale can be used for mass production of devices, and each pattern is engaged as a single device [70]. E-beam lithography, on the other hand, is capable of producing fine structure arrays with smaller scales and more precise demands since its diffraction limit is much smaller than ultraviolet radiation [100]. It is well known that focused ion beam (FIB) is a powerful patterning tool as a 'nano-cutter'. Moreover, FIB is capable of producing nanomembrane kirigami or metasurface structure by cutting and bending nanomembrane in one processing step—when nanomembrane is exposed to ion irradiation, the produced vacancies and the implanted ions may introduce residual strain for sophisticated assembly [101]. This will be detailly discussed later.

Reactive ion etching (RIE) and wet chemical etching processes can then create patterns on the given nanomembrane beneath the resist layer. In the RIE process, the exposed region of nanomembrane can be removed by the attack and reaction of high energy ions from gas plasma produced by electromagnetic fields [102]. The high kinetic ions and reaction build good vertical sidewalls perpendicular to the etching edge [99]. There are cases where wet chemical etching is used for its cheap cost and easy process [103, 104]. However, wet chemical etching in some cases was not the preferred choice because it may bring severe undercutting underneath the nanomembrane to break the pattern [105]. In fact, patterning can be realized without etching. After the lithography process brings an inverse pattern fabricated on the resist layer, intended materials can deposit on the exposed region on the substrate [106], which fabricates patterned nanomembranes. However, these methods are not suitable for materials that are deposited at high temperature because of the poor heat resistance of the resist layer.

Another necessary process for fabricating 3D structure is releasing nanomembrane step (figure 2(c)), after which nanomembranes will lose the attachment to the substrate and become freestanding. The most common method to release the nanomembrane from the substrate is to insert a sacrificial layer between the nanomembrane and substrate, and then remove the sacrificial layer. The etchants are limited by the request of high etching selectivity for the sacrificial layer, while both solution and vapor can be used as etchants in different systems. For instance, the sacrificial layer of heavily doped n-type GaN (Si-doped) nanomembrane is selectively etched by HF solution while the above undoped GaN is kept intact [102]. HF solution can also be used to etch SiO_2 sacrificial layer, which is widely used to produce 3D optoelectronics devices on Si substrate [65]. Except for releasing Si nanomembranes, HF solution is adopted to separate the composite layer like graphene/polymethyl methacrylate from SiO_2/Si substrate [107]. On the other hand, H_2O_2 solution can be used to release nanomembrane on Ge sacrificial layer [61]. More, an organic solvent (such as acetone) is utilized to remove the photoresist sacrificial layer, and the selection of substrate and nanomembrane can be remarkably broadened because the high selectivity of organic solvent makes the approach applicable for almost any inorganic materials [106]. Except for the wet methods of etching, dry etching such as vapor can also react with the selected sacrificial layer and release the nanomembrane. For example, HF vapor was used to remove the SiO_2 layer while Si and graphene layers were well protected [108], and XeF_2 vapor can etch semiconductor layer to release the SiN_x and metal multilayer [109, 110]. Generally, wet method is a cheap and easy method but easy to corrode the surface of the wanted nanomembrane, while dry method is expensive and complex but with better selectivity of sacrificial layer [111]. It is worth noting that in order to assist the release process, a transfer printing method may be applied. During transfer printing, an elastic stamp is typically used to transfer nanomembrane onto a target substrate [112]. Studies have demonstrated that the transfer printing of nanomembranes can help in assembling nanomembranes and constructing photonic and optoelectronic devices on desired supporting substrates [113–115].

2.3.3. 3D assembly of nanomembrane. Nanomembrane-based assembly techniques can usually prepare complex 3D micro/nano structures through a variety of detailed approaches (figure 2(d)), such as rolling, folding, buckling and pick-place assembly [116].

By designing residual strain difference/mismatch between layers, nanomembrane can be rolled up into tubular structures (figure 2(d)-(i)) like microtube [35, 117] or helix [31, 118]. During the rolling process, strain mismatch generates enough driving force to overcome the resistance and provide the motivation for rolling until the length of needed turns. Rolled-up nanomembranes typically consist of two layers of material with different structures/lattice constants to provide the needed vertical strain gradient. For example, materials with different lattice constants deposit in order, and the lattice constant of the upper layer is greater than that of the lower layer [119]. Thus, the upper layer material is compressed along the in-plane direction and the lower layer material is tensile. The interatomic forces between the two layers are in opposite directions, so the moment to roll up the bilayer can be obtained when the bilayer nanomembranes are released from the substrate. For relatively thin bilayer nanomembranes, this method allows precise control of the bending moment based on the lattice constant, which means that mismatch strain can be introduced and tuned by choosing different materials. Various semiconductor materials have been explored as choices, including materials in IV [120], III–V [121] and II–VI [122] groups, offering a variety of options for strain modulation. As the strain status in the nanomembrane is crucial for the rolling assembly, several other strategies were also developed to introduce the strain and corresponding difference, such as tuning the parameters during the deposition process [106] and adding active layers [123]. The construction of tubular microstructures with rolled-up techniques can be precisely controlled by several factors, like processing parameters, material properties and nanomembrane geometry [29, 124]. For instance, helical microstructures can be realized by rolling stripe-shaped nanomembrane [31, 125, 126].

The folding process generally refers to folding relatively rigid nanomembranes to the desired angle through local bending deformation (figure 2(d)-(ii)). The driving forces of folding include external forces such as capillary forces and internal forces caused by strain mismatch. It was reported that folding induced by capillary force relies on the surface tension generated by droplets or fusible hinges to drive the assembly, with considerable strength [30, 127, 128]. Precise control of folded assemblies is achieved by introducing residual stress into localized regions to form hinges. Another typical method to accurately generate gradient stress along the nanomembrane thickness is FIB, which can introduce voids at the hinge and fill the voids with implanted high-energy ions, resulting in folding deformation to release the compressive stress at the hinge [129, 130]. By precisely controlling compressive and tensile forces, folding methods can be used to prepare nanomembrane origami/kirigami with fantastic 3D micro/nano structures with the potential for optical regulation [127, 129, 130].

The buckling assembly method mainly applies to the deformable substrate [131], which can provide a mechanical force to drive the 3D assembly (figure 2(d)-(iii)). Wavy [132], pyramidal [133] and coils [131] structure can be constructed by buckling assembly through the process including 2D pattern fabrication and mechanical clasping. Specifically, the 2D patterned nanomembrane is built by planar lithography techniques, and the selective binding sites are introduced by covalent binding [112]. In figure 2(d)-(iii), the outer squares are connected to rectangular anchors firmly adhered to biaxial prestrained elastomer substrate. By eliminating the sacrificed interface layer, all other areas are released from the substrate. Relaxation of prestrain produces compressive strain that causes the structure to bend out of the plane, and the 2D patterned nanomembrane is transformed into the designed 3D geometrical structure [134]. The key factors of buckling assembly include patterns of nanomembrane, strain distribution of supporting substrates and the way of strain release. By carefully considering these factors, micro/nano structures can be deterministically assembled.

The pick-place method (figure 2(d)-(iv)) is mainly used to produce the integrated optoelectronic device/system with nanomembrane origami/kirigami geometry and a typical example is an electronic eye system with curved 3D surfaces [55, 135], In pick-place approach, traditional planar transfer printing technique is combined with curved elastic substrates to form non-planar device/system with unconventional properties and functions [134]. It is worth noting that this non-planar transfer printing is also applicable to rigid template [136, 137]. Since micro/nano devices are often fabricated by using planar lithography, so the development of new transfer printing techniques plays an important role in 3D assembly [138, 139].

It is worth mentioning that several induction effects may facilitate the deformation of nanomembrane and the construction of 3D assembly. For instance, the nanomembrane can be deformed by capillary force produced by the phase change of trigger materials set on the prescribed position of nanomembrane [30, 127, 128]. In addition, physical or chemical reactions in active materials can also induce forces between the interfaces of multilayered structures similar to the residual strain, triggering 3D assembly [140]. While in the case of nanomembrane kirigami, substrate engineering is important as well [141].

3. Application of assembled nanomembrane in nanophotonics and optoelectronics

Due to the unique properties different from bulk materials, various photonic and optoelectronic devices by assembling nanomembranes have been fabricated. Especially, 3D structures based on the assembled nanomembrane will bring devices different performances compared to the ones based on bulk materials with flat configuration. Table 1 summarize versatile 3D nanomembrane-assembled structures. It can be seen that from optical regulation to sensing, 3D assembled nanomembranes are widely used for various applications in nanophotonics and optoelectronics. In the following sections, typical applications will be summarized and reviewed.

Table 1. Summary of nanomembrane assembled structures for applications in nanophotonics and optoelectronics.

Assembly approaches	Materials	Assembled structures	Device applications
Rolling	Si	Microtube	Photodetector [70]
	SiO/SiO_2	Microtube	Humidity sensor [69]
	ZIF-8-Y_2O_3/ZrO_2	Microtube	Gas sensor [146]
	Cr/Au	Microtube	DNA sensor [147]
	PCM	Microtube	Optical resonator [148]
	InGaAs/InGaAsP QWs	Microtube	Laser [149]
	Graphene	Microtube	Field-effect transistor [150]
	VO_2-based	Helix	Optical switch [31]
Folding	Au/SiN_x	Double asymmetric rings	Photon-spin selective device [28]
	Cu	Miura-Ori	Chirality tuner [151]
	Au/Al_2O_3	Nanocube	Optical resonator [152]
	Au	Double-plate-based	Optical resonator [153]
	Au/SiN_x	Handed-like	Optical switch [154]
	MoS_2/Au	Flower-like	Photodetector [155]
Buckling	MoS_2 /Graphene	Octagonal prismoid/hemispherical	Photodetector/image sensor [49]
	Ti/SiO_2	Ribbons	Photodetector [156]
	Ge	Wrinkle	Photodetector [157]
	Au/SU8	Pyramidal	Mechanical tunable optical transmission window [133]
	Au (Ag/Al)/Ti/ SiO_2	Wavy	Plasmonic structure [158]
	CNT/PVA	Nanonet	Diffraction grating [159]
	Au	Pinwheel	Optical reconfiguration [160]
	Au/SiN_x	Helix	Optical chirality sensing [161]
Pick-place	Au	Hemispherical	Artificial eye system [135]
	MoS_2 /Graphene	Hemispherical	Artificial eye system [55]
	Si	Hemispherical	Artificial eye system [162]
	Si/ARC	Curved	Phototransistor [18]
	Si	Flexible	Microwave transistors [163]
	Liquid crystal	Skin-like	Thermal sensor [164]
	Si	U-shaped	Transient biosensor [137]
	InGaP/InGaN	Stripe	light emitting diode (LED) biosensor [165]
	Au	Nanohole	Plasmonic sensor [166]

3.1. Whispering gallery mode microcavity based on rolled-up nanomembrane

Based on various modes of light confinement, three groups of optical microcavities are defined as Fabry–Pérot microcavity [142], photonic crystal microcavity [143] and whispering gallery mode (WGM) microcavity [144, 145]. Fabry–Pérot cavity which confines light between two planar and parallel mirrors is the simplest form. Microcavities based on photonic crystals can provide extremely small mode volumes. WGM resonance was first observed and studied in the acoustic mode of St. Paul's Cathedral. The study of WGM gradually expanded to the field of optics.

Previously, WGMs resonators are typically dielectric spherical structures. With the maturation of rolled-up nanomembrane strategy, the microtubular structures fabricated by rolled-up technique have been widely used as tubular WGM resonators, which exhibit effective light confinement via resonance, leading to enhanced light–matter interaction [167]. The wave equation of tubular microcavity can be described by cylindrical coordinates as shown in figure 3(a). Due to the open characteristic of hollow tubular microcavity, the WGM can be considered as a quasibound state with time decaying exponentially [168]. Defining the WGM as a time-harmonic solution of Maxwell equation with vector k, the wave equation is

$$-\frac{1}{n^2(r,\varphi,z)}\nabla^2\vec{E}(r,\varphi,z)=k^2\vec{E}(r,\varphi,z) \quad (1)$$

where n represents the position-dependent refractive index of the tube material, k represents the vacuum wave vector. In the case that the thickness of rolled-up nanomembrane is much smaller than the resonant wavelength, WGMs with transverse-magnetic (TM) -polarization are dominated. Transverse-electric-polarized mode is absent until the wall thickness reaches a critical value [169].

With the improvement of rolled-up nanotechnology, versatile materials have been prepared for rolled-up tubular nanomembranes as WGM optical microcavities [170]. The reported materials include semiconductor [171], diamond [172], metal [147], oxide [69], 2D materials [26], etc. Compared with planar nanomembrane, the light emission of microtube at resonant wavelength is significantly enhanced due to the special light confinement effect in the tubular structure. Polarization of the light propagating the rolled-up nanomembrane can also be remarkably influenced by the 3D tubular geometry [173, 174]. The technology of rolling planar

nanomembranes avoids complex surface processing to obtain complex 3D structure [31], because by utilizing the graphic technology of Si plane process, nanomembranes of different shapes can be rolled-up [175]. The flexibility in materials adopted in rolling assembly leads to unique optical properties in the microtubular cavity. For example, the diamond cavity was considered as a great candidate for the efficient generation of quantum carriers in the color centers [172]. By designing the rolled-up diamond nanomembrane, a rolled-up diamond microcavity with high quality factor (Q factor) was formed [172]. On the other hand, based on rolled-up metal nanomembrane, hybrid modes with both subwavelength confinement and high Q factor can be supported by the optoplasmonic WGM microcavity [176]. Rolled-up oxide nanomembrane with spiral cross-section is capable of producing 3D directional light emissions [177]. So far, the mature fabrication process of the rolled-up nanomembrane provides the possibility of 3D optical regulation by adjusting the geometry which is quite hard for planar optical structure [178–180]. It is worth noting that the rolled-up microcavity owns strong optical resonance mainly due to the ring-like cross-section [181]. However, rolled-up microcavities are different from normal ring resonators, because light confinement along axial direction exists, demonstrating a unique 3D light tunability [182, 183].

Previously, the modification on geometric factors (including the edge, the overlap length, and asymmetry of nanomembrane) of the rolled-up nanomembrane was used for light regulation [177, 184]. As shown in figure 3(b)-(i), Wang *et al* [177] proposed that the lobe of rolled-up SiO/SiO_2 nanomembrane causes different turns on every position of spiral cross-section, which can achieve directional light emissions, due to interaction between 3D optical resonances and lobe edge. Figure 3(b)-(ii) shows the relation of calculated unidirectionality U versus winding number W for TM mode, which reveals the transition of bi- and unidirectional emission states is tunable by adjusting the cavity confinement and mode chirality. For the rolled-up microcavities fabricated from patterned nanomembrane, their optical properties can be further controlled by the edge of nanomembrane. Fang *et al* [184] specifically researched the changing of resonant modes with the increase of overlap length between the spiral notches (figure 3(c)-(i)), and noticed the changes in resonant wavelength and Q factor (figure 3(c)-(ii)). On the basis of theoretical simulation, the modulation behavior of Q factor is considered to be caused by the strong interactions of scattered waves between the spiral notches [171]. In addition, the asymmetric structure of the microtube, deviating from the standard cylindrical shape, will also cause changes in optical resonance. Quinones *et al* [185] investigated confined optical resonance in 3D asymmetric microtube fabricated by uneven rolled-up SiO/SiO_2 nanomembranes, of which the radii increased along the axial direction as shown in figure 3(d)-(i). By altering microtube radii and refractive index of tube wall, axial modes can be indicated by the horizontal dashed lines with a larger spacing in figure 3(d)-(ii), which implies enhanced axial confinement.

Furthermore, various fine structures constructed on the nanomembrane (i.e., tube wall) are also reported to be able

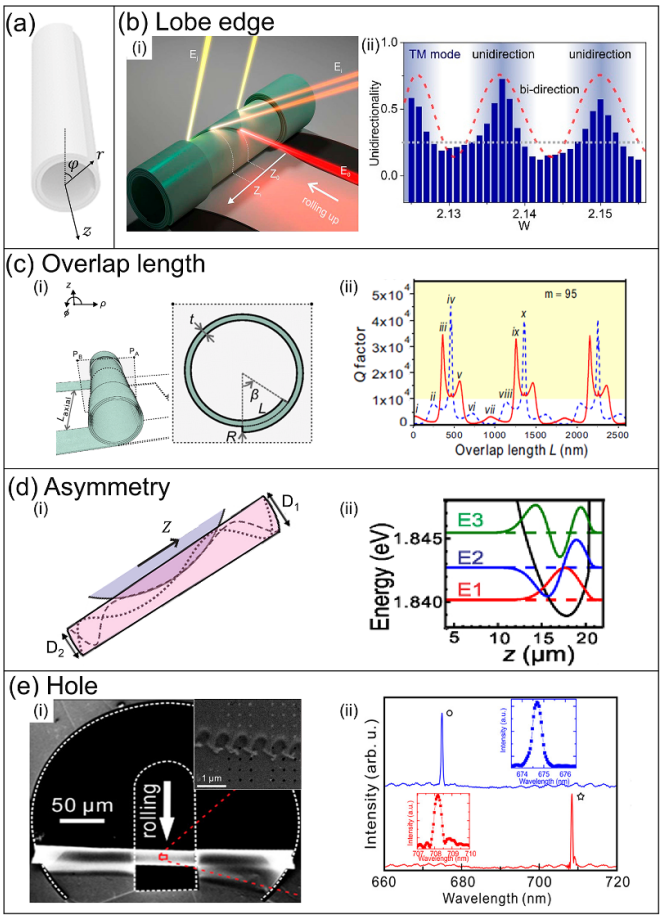

Figure 3. Optical tuning in rolled-up microcavity. (a) Schematic of a rolled-up tubular nanomembrane microcavity defined with cylindrical coordinate. (b) Optical resonant mode regulation by lobe edge of microtube [177]. Reprinted with permission from [177]. Copyright (2019) American Chemical Society. (i) Schematic of rolled-up spiral-shaped oxide microcavity. (ii) Calculated unidirectionality versus winding number for TM mode. (c) Modulation of Q factor in rolled-up microcavities by the edge of nanomembrane [184]. Reprinted (figure) with permission from [184], Copyright (2016) by the American Physical Society. (i) Schematic of the cross section showing structural notches and overlap of the nanomembrane. (ii) Evolution of Q factor as the overlap length increases. (d) Rolled-up microcavity with asymmetric structure for axial confined optical resonance [185]. Reprinted with permission from [185] © Optica Publishing Group. (i) Schematic of rolled-up asymmetric microtube. (ii) Axial field distributions for first three modes. (e) Single-mode emission in rolled-up microcavity with hole array [172]. Reprinted with permission from [172]. Copyright (2018) American Chemical Society. (i) Scanning electron microscope (SEM) image of the rolled-up diamond microcavity with periodic hole array on the wall. (ii) Light emission spectra of microtubes with different hole arrays.

to tune the optical properties of rolled-up microcavity. For example, surface plasma structures on the tubular optical microcavity are expected to improve Q factor, and change the polarization characteristics of the resonance [186]. Further studies have shown that surface plasmas can be coupled not only with the conventional WGM mode, but also with the axial mode to change the 3D regulation ability of microtubular structures [187]. In order to further demonstrate the

3D photonic tuning ability of the rolled-up microcavity, Tian *et al* [172] fabricated a photonic crystal structure of period hole array on the tube wall by micro/nano fabrication technology, as shown in figure 3(e)-(i). The mode selection can be realized through the coupling of distributed feedback effect from photonic crystal and WGM mode, so as to achieve the purpose of single mode emission. Different geometries (e.g., periodicities of array and radii of holes) lead to the single-mode emission at different wavelengths (figure 3(e)-(ii)). The unique rolling geometry is also expected to make breakthroughs in the optical chiral regulation by combining the advantages of the phase-modulation mechanism and WGM resonance [172]. Fishnet-like tube wall was also reported to produce optical microcavity with a negative refractive index and high Q factor [188]. Moreover, detailed research shows that the nanogaps in the tube wall between adjacent rotations lead to the split of resonant mode and several sets of 3D confined resonant modes can be observed [189]. The research on how the interlayer nanogap affects the optical properties provided a guideline for the future design and fabrication of rolled-up microcavity [190].

There are many other ways to regulate the rolled-up microcavity and change the resonant wavelength and/or Q factor. The subwavelength-thickness of rolled-up nanomembranes leads to a strong evanescent field with serve leakage, and thus the resonance characteristics of rolled-up nanomembrane are easier to be shifted under the change from the refractive index of the surrounding medium. Thus, in addition to structure-based optical regulation, sensitive optical sensing applications may also be realized by tuning light–matter interaction. For example, Huang *et al* [69] prepared a rolled-up SiO/SiO_2 bilayer nanomembrane with subwavelength wall thickness which has an important application in optofluidics for real-time sensing. Miao *et al* [191] also reported a rolled-up microtube containing QDs as a microfluidic device (figure 4(a)-(i)). WGMs are enhanced due to the evanescent field coupling of the QDs with the rolled-up resonator. The device can be applied in sensing applications because the wavelength shifts are dependent on the evaporation of the solvents. Figure 4(a)-(ii) shows that polarized light (PL) spectra of a blank SiO/SiO_2 microcavity, Cd_3P_2 QDs, and those filled with the Cd_3P_2 QDs during the solvent (toluene) evaporation, and obvious mode shift can be observed. In addition, since the rolled-up WGM microcavity produces resonance from the incident light, the working wavelength of the microcavity may also be tuned by evanescent coupling. Lin *et al* [192] reported a rolled-up microcavity made from poly diallyldimethyl ammonium chloride (PDDA)/in poly acrylic acid (PAA) bilayer nanomembrane where Rhodamine 6G (R6G) dye molecules were incorporated in the tube wall (figure 4(b)-(i)). The photoluminescence at a certain wavelength from the dye molecules was effectively coupled with WGM resonance to adjust the operating wavelength, as shown in figure 4(b)-(ii).

As mentioned above, the interaction of the evanescent field between the optical resonance and the medium near the tube wall (inner and outer regions) results in the shift of the resonant wavelength [69, 193]. Active materials with different functionalities can also be incorporated to modify optical properties of rolled-up microcavity, fulfilling different sensing tasks, and thus more application potentials of rolled-up microcavity can be expected. In figure 4(c)-(i), Yin *et al* [26] demonstrated a rolled-up optical microcavity modified with precious metal and graphene layers sequentially on the surface. The electric field of hybrid optoplasmonic modes at the cavity surface is significantly enhanced by the addition of a graphene layer, and the shift of resonant mode is remarkably increased. This brings a highly sensitive surface detection power at sublayer level (figure 4(c)-(ii)). However, it is difficult for optical microcavity to detect gas molecules because of the tiny refractive index variation and the fact that gas molecules cannot effectively gather around the tube wall. Therefore, researchers managed to introduce specific functional materials onto the rolled-up nanomembrane to 'collect' the gas molecules. Zhang *et al* [193] proposed an oxide tubular microcavity that is decorated by PAA/PEI polymer layer via layer-by-layer approach (figure 4(d)-(i)). In this work, humidity sensing is realized on the basis of the absorption of water moisture in the polymer layers, and the swelling of the polymer layer leads to the change in the geometry of the microcavity. Figure 4(d)-(ii) shows the mode shift caused by the absorption of moisture.

Yang *et al* [117] introduced Pd NPs on the surface of the rolled-up tubular structure (figure 4(e)-(i)). As a functional material, Pd NPs are utilized to absorb hydrogen molecules and their refractive index changes correspondingly. The modified optical microcavity can therefore be applied in highly sensitive hydrogen detection (figure 4(e)-(ii)). Kong *et al* [146]reported that metal-organic framework (MOF) layer also can be deposited onto both inner and out surfaces of tube wall to enhance selective gas absorption due to the nanoporosity of MOF layer (figure 4(f)-(i)). Figure 4(f)-(ii) shows that the rolled-up microcavity modified by MOF layer is effective in CO_2 sensing, and the WGM wavelength shifts linearly with CO_2 concentration [146].

To sum up, the researches on WGM microcavities based on rolled-up nanomembranes focus on understanding and tuning the optical properties. More applications may be expected in the future by elaborated optical tuning in microtubular cavities incorporated with functional materials.

3.2. *Lasing based on rolled-up microcavity*

As mentioned in the above section, rolled-up microtubular nanomembranes take the advantage of enhancing light–matter interaction, providing a potential probability for lasing [194]. Due to the unique geometric structures, the lasers based on rolled-up microtubular structures are expected to possess good controllability on polarization and emission direction [47].

Under optical pumping, the threshold power may be high compared to that in microdisk laser or photonic crystal laser, because the surface to volume ratio of microtube is large. Therefore, electrical injection can be an alternative option in some situations. In previous researches, by adding QDs as gain materials and emitters, lasing can be obtained at room temperature in rolled-up devices. In figure 5(a)-(i),

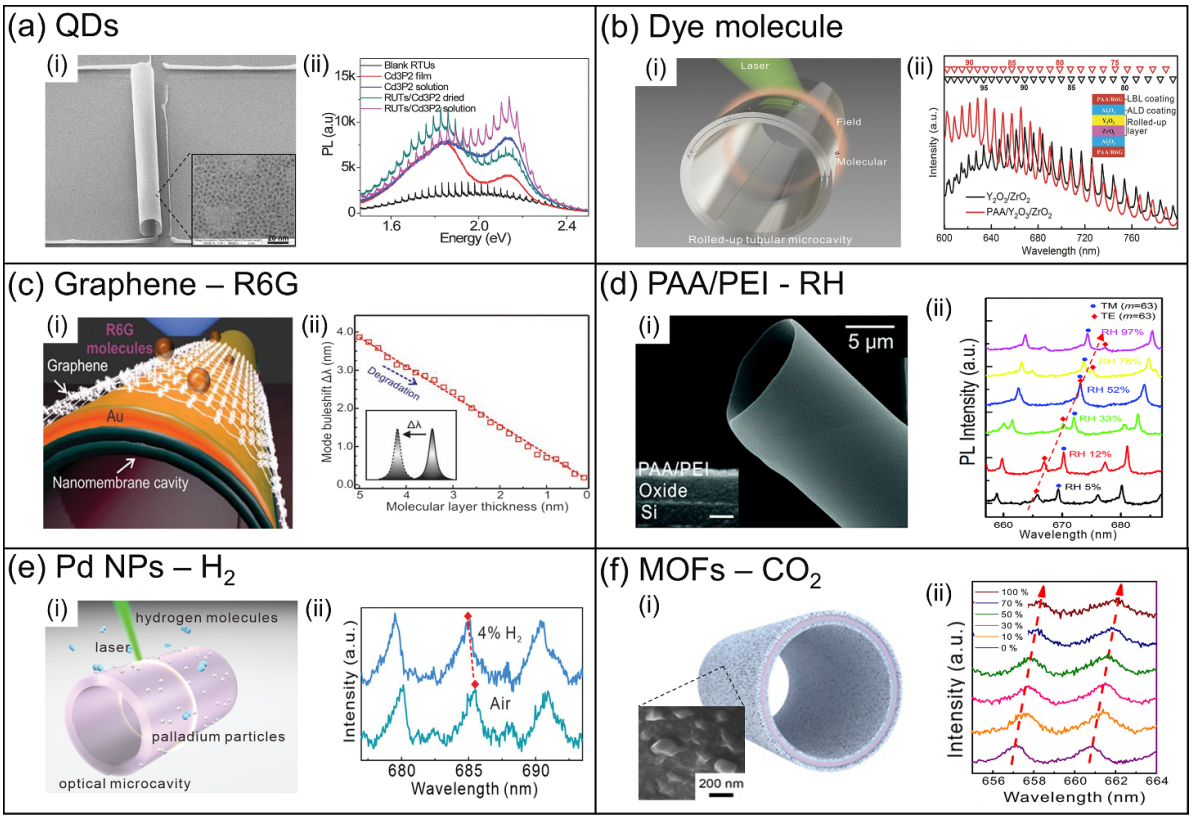

Figure 4. Rolled-up microcavity incorporated with functional materials for sensing application. (a) Rolled-up microtube decorated with QDs as optofluidic sensor [191]. [191] John Wiley & Sons. [Copyright © 2015 WILEY-VCH Verlag GmbH & Co. KGaA, Weinheim]. (i) SEM image of rolled-up microtube containing Cd_3P_2 QDs. (ii) Light emission spectra of the blank microtube and QDs embedded microtube before and after solvent evaporation. (b) Tuning of resonant wavelength by dye molecules coupling [192]. [192] John Wiley & Sons. [Copyright © 2016 WILEY-VCH Verlag GmbH & Co. KGaA, Weinheim]. (i) Schematic of rolled-up microcavity incorporated with dye molecules. (ii) Light emission spectra collected from the tubular microcavity before and after incorporation of dye molecules. (c) Optical microcavity modified with graphene layer to detect R6G molecules [26]. Reprinted with permission from [26]. Copyright (2019) American Chemical Society. (i) Schematic of resonant light field interacting with the R6G layer on graphene. (ii) Calculated mode shift (inset) as a function of the R6G molecule layer thickness. (d) Rolled-up polymer/oxide/polymer microcavity for humility detection [193]. Reproduced from [193] with permission from the Royal Society of Chemistry. (i) SEM image of rolled-up PAA/PEI/oxide nanomembrane. (ii) PL spectra from PAA/PEI modified microcavity in atmospheres of different humidities. (e) Rolled-up tubular microcavity modified by Pd NPs for hydrogen detection [117]. [117] John Wiley & Sons. [Copyright © 2022 WILEY-VCH Verlag GmbH & Co. KGaA, Weinheim]. (i)Schematic of Pd NPs-decorated Y_2O_3/ZrO_2 microtube (ii) Emission spectra of the microcavity placed in air and 4% H_2. (f) MOF layer modified rolled-up microcavity for CO_2 detection [146]. Reprinted with permission from [146]. Copyright (2021) American Chemical Society. (i) Schematic of the Y_2O_3/ZrO_2 microtube decorated with MOFs layer (The inset is the corresponding SEM image). (ii) Light emission spectra from the MOF modified rolled-up nanomembrane in the atmosphere with different CO_2 concentrations.

InGaAs nanomembrane containing GaAs QDs is released to build a microtube from GaAs substrate by selectively etching AlAs sacrificial layer [195]. The rolled-up nanomembrane can achieve a high Q factor laser, which can be pumped optically with a minimum intrinsic linewidth of ∼0.2–0.3 nm and a low threshold of ∼4.0 μW at room temperature, as shown in figure 5(a)-(ii). Moreover, InAs QDs are also incorporated in rolled-up InGaAsP nanomembrane as the gain materials [47]. In addition to QDs, QWs can be adopted as gain materials as well. In figure 5(b)-(i), InGaAs/InGaAsP QWs heterostructure forms an electrically injected rolled-up microtube laser [149]. The evaluation of background emission at different currents confirms the lasing behavior at the telecom wavelength range above the threshold current of ±1.05 mA (figure 5(b)-(ii)). It is worth noting that such rolled-up structures could be readily transferred onto Si substrates and applied in chip-level optical communication systems as a coherent light source.

We believe that 3D rolled-up structure opens up new possibilities for tunable emission directionality, which may be of great benefit in fundamental studies and applications.

3.3. *Microtubular photodetector*

Efficient light detectors are the main requirements of modern scientific technology, and light detection is the basis for emerging application fields such as near-infrared medical imaging, visible light cameras and machine vision. Photodetectors are capable of converting photons of different energies into electrical signals for subsequent processing, image reconstruction and storage. The performance of photodetector depends on the absorption of light by materials. Therefore, the key to improving the performance of photodetector is to enhance the interaction between light and materials. At present, the addition of functional material and construction of optical

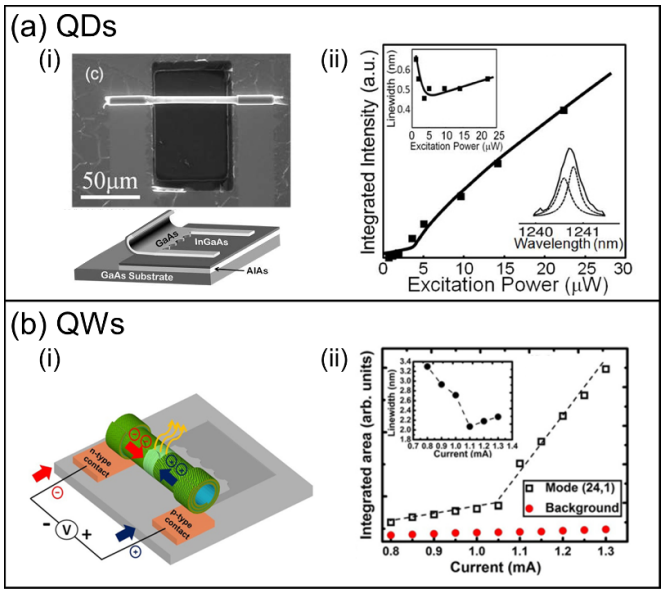

Figure 5. (a) Optically pumped rolled-up InGaAs/GaAs QDs microtube lasers [195]. Reproduced from [195]. CC BY 4.0. (i) Schematic and SEM image of the device. (ii) Integrated emission intensity and linewidth (inset) of the mode versus pump power. (b) Electrically injected rolled-up InGaAs/GaAs QDs microtube lasers [149]. Reprinted from [149], with the permission of AIP Publishing. (i) Schematic illustration of the device. (ii) Integrated emission intensity and linewidth (inset) of the mode versus current.

structures are common approaches. Recent studies show that 3D photodetectors are possible to form a light-field regulation structure on a larger scale than metal grating as well as surface plasma, and light and semiconductor materials interaction increases remarkably [196, 197]. Among various 3D microscale structures, tubular devices have received more and more attention. The photon regulation capability endows the corresponding photodetector with higher sensitivity and omnidirectional detection ability, superior to their planar counterpart [11, 70, 150, 198–201].

Due to the high quality optical response, semiconductor nanomembranes are widely used to manufacture photodetectors [22]. Figure 6(a)-(i) shows a 3D tubular photodetectors constructed by rolling Si nanomembrane as an example [70]. A significant increase in photocurrent and decrease in dark current can be observed in rolled-up photodetector (figure 6(a)-(ii)). The characterization shows that the light switching ratio of the rolled-up photodetector is enhanced to 10^3 times that of the planar structure, due to the enhanced optical coupling and the suppression of dark current. The mechanism of dark currents suppression in rolled-up nanomembrane structures can be attributed to two possible factors: the increase in the surface charge capture state and the piezoresistive effect. High density surface state can generate at the inner and outer surfaces of the tube wall acting as a charge trap [202, 203]. In addition, the increase in surface state and roughness caused by the rolling process of Si nanomembrane can serve as an effective absorption source, further improving the device's performance [36]. QWs are embedded in semiconductor nanomembrane for enhanced sensing in a certain wavelength range. Wang *et al* [11] reported a 3D infrared photodetector by rolling up GaAs/AlGaAs QWs nanomembrane (figure 6(b)-(i)). Due to the internal reflection trap effect, the photocurrent response of the rolled-up microtubular device in the wavelength range of 3–8 μm is more than three times higher than that of the planar device (figure 6(b)-(ii)), and the number of rotations in the tube wall can be used to further regulate the response rate. In addition, the rolled-up microtubular structure provides a nature optocoupler path without the external optocoupler structure that is typically required by QWs photodetector. This 3D infrared photodetector device provides a unique solution for high performance infrared focal plane arrays as an 'omnidirectional' detector, obtaining efficient infrared detection at a wide angle of incidence ($\pm 70°$). In addition, it is found that in rolled-up QWs nanomembrane, the tensile and compressive statuses obviously influence the photoresponsivity. Quantitative investigation shows that QWs nanomembrane in tensile status can enhance the photoresponse by about 2.1 times, and QWs nanomembrane in compressive status leads to a decrease of photoresponse to $\sim$65% [204].

2D materials are also applied in 3D rolled-up photodetectors. In particular, as a 2D material, MoS_2 is capable of detecting a wide range of spectrum from visible to infrared regions with high carrier mobility and tunable bandgap [173, 174]. The characterization of the 3D rolled-up device shows that the photocurrent increases linearly to the light intensity, exhibiting good sensitivity. Figure 6(c)-(i) shows that MoS_2 nanomembranes are integrated on an optically transparent substrate to form a rolled-up photodetector [27]. It is demonstrated that the 3D rolled-up photodetector exhibits a faster response time and stability, as shown in figure 6(c)-(ii). In addition, graphene has superior electronic and optical properties for photodetector, but the photoresponsivity of corresponding planar photodetector is also limited by weak optical absorption. To enhance the photodetection performance, Deng *et al* [150] proposed 3D tubular graphene field-effect transistors by rolled-up methods (figure 6(d)-(i)). After assembly, the photoresponsivity of the 3D tubular photodetector is significantly increased to 1 AW^{-1} in visible and ultraviolet regions (figure 6(d)-(ii)), which is attributed to the enhancement of the optical field and the expansion of light-graphene interaction area.

With the development of fabrication technology and application of materials, the 3D microtubular photodetectors can be used in more diverse conditions and environments. Predictably, photodetectors based on 3D structures are considered to have great potential.

3.4. Optical device based on nanomembrane origami/kirigami

Since their scales are comparable with light wavelength, the nanomembrane origami/kirigami has expanded their application fields from mechanics and acoustics to nanophotonics. With the development of 3D assemblies of nanomembranes, their unconventional optical properties have been explored for applications in nanophotonics and optoelectronics.

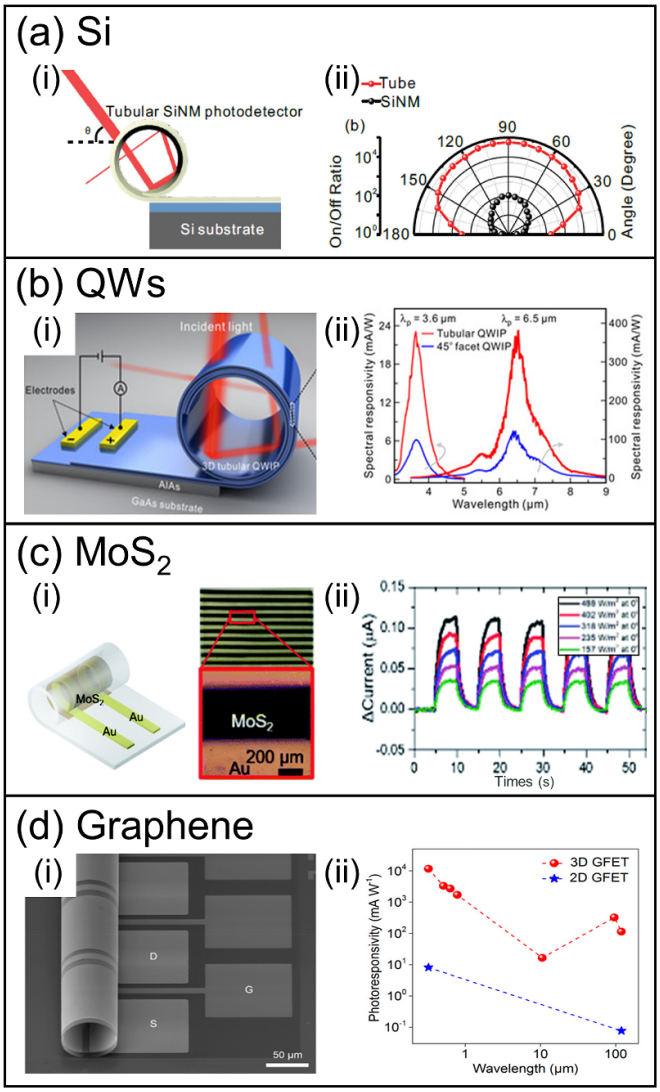

Figure 6. Rolled-up microtubular photodetector. (a) Rolled-up Si nanomembrane in a tubular geometry for enhanced photodetection [70]. [70] John Wiley & Sons. [Copyright © 2019 WILEY-VCH Verlag GmbH & Co. KGaA, Weinheim]. (i) Schematic illustration of tubular photodetector. (ii) Comparison of on/off ratios of rolled-up photodetectors and planar device. (b) Rolled-up QW nanomembranes for high performance photodetector [11]. Reproduced with permission from [11]. CC BY-NC 4.0. (i) Schematic illustration of the 3D device. (ii) Spectral responsivities of 3D microtubular photodetector and corresponding planar device. (c) Rolled-up photodetector based on MoS_2 nanomembrane [27]. Reproduced from [27] with permission from the Royal Society of Chemistry. (i) Schematic illustration of rolled-up MoS_2 nanomembrane for photodetection. (ii) Photocurrents as a function of time under periodic illumination with varying illumination intensities. (d) Rolled-up graphene transistors as photodetector [150]. Reprinted with permission from [150]. Copyright (2019) American Chemical Society. (i) SEM image of a typical 3D graphene field-effect transistor. (ii) The photo responsivity of planar and rolled-up transistors.

The unique twisting structure in nanomembrane origami/kirigami which is out of the plane has the potential to generate unique electromagnetic properties, such as 3D optical chirality [101, 205]. Intrinsic chirality refers to geometric properties of 3D structures without the mirror symmetric plane. Artificially designed chiral structures can observe stronger optical chiral responses than in natural materials, because there are huge mismatches between the characteristic size of atoms and the wavelength of light [206, 207]. In 2D planar structures, extrinsic optical chirality can be observed by a relatively weak response due to the condition of a strict oblique incident angle [208]. Optical chirality derives from the cross-coupling between electric and magnetic dipoles in the parallel direction [209], and the perpendicular direction of induced magnetic dipole and electric dipole decouples and weakens optical chirality in 2D planar structures. Therefore, 3D nanomembrane assembly with features in the direction of propagation, such as pinwheels [101], vertical helices [205] and folded metasurfaces [28, 153] are highly desirable for obtaining strong optical chirality. The feasibility and diversity of nanomembrane assembly make corresponding 3D origami/kirigami assembly attractive for this field.

FIB is the most common method used to fabricate kirigami structures by cutting and bending nanomembrane to generate 3D geometries. For example, figure 7(a)-(i) shows 3D pinwheel array fabricated on gold nanomembrane which can explore versatile optical manipulation for phase and polarization [101]. 3D twisted structure in pinwheel array induces the parallel electric and magnetic moments, which brings giant intrinsic optical chirality. Enhanced variation of circular dichroism (CD) effects and giant polarization versus wavelength is shown in figure 7(a)-(ii). With left-hand (LH) and right-hand (RH) 3D pinwheels, the binary diffractive grating can be manufactured by patterning metasurfaces with opposite handedness in order. The 3D pinwheel structure shows a preferable performance in the enhancement of optical chirality compared to the inconspicuous phenomenon in chiral 2D patterns [210]. More importantly, these 3D nanostructures based on kirigami assembly successfully expand the working wavelength to visible region [211]. Figure 7(b)-(i) shows a 3D Archimedes spirals array constructed by pulling out from the stacked nanomembranes cut by FIB [161]. The 3D Archimedean spiral structure based on kirigami nanomembrane is a self-similar chiral fractal structure sensitive to the chirality of light. Fabricated 3D metasurfaces show extraordinary chiral asymmetry with stable and enhanced optical chirality. Under the excitation of circularly polarized light including right-handed circularly polarized and left-handed circularly polarized, excellent chiral dissymmetry in transmission and near-field broadband response at the wavelength of 2–8 μm is exhibited in the 3D spiral structure (figure 7(b)-(ii)). Uniform and highly enhanced broadband near-field optical chirality is generated at a stable local position in the spiral with linearly polarized excitation [161].

Chiral metasurface of folded nanomembranes can be utilized for light manipulation including the selection of spinning and tuning of resonance. For example, in figure 7(c)-(i), Yang *et al* [28] manufactured a chiral folded metasurface consisting of an antisymmetric split-ring resonator (SRR) array that is capable of light spin-state selection. Since the mirror symmetry is broken, electric and magnetic dipole resonances are strongly coupled. Owing to the prominent intrinsic chirality,

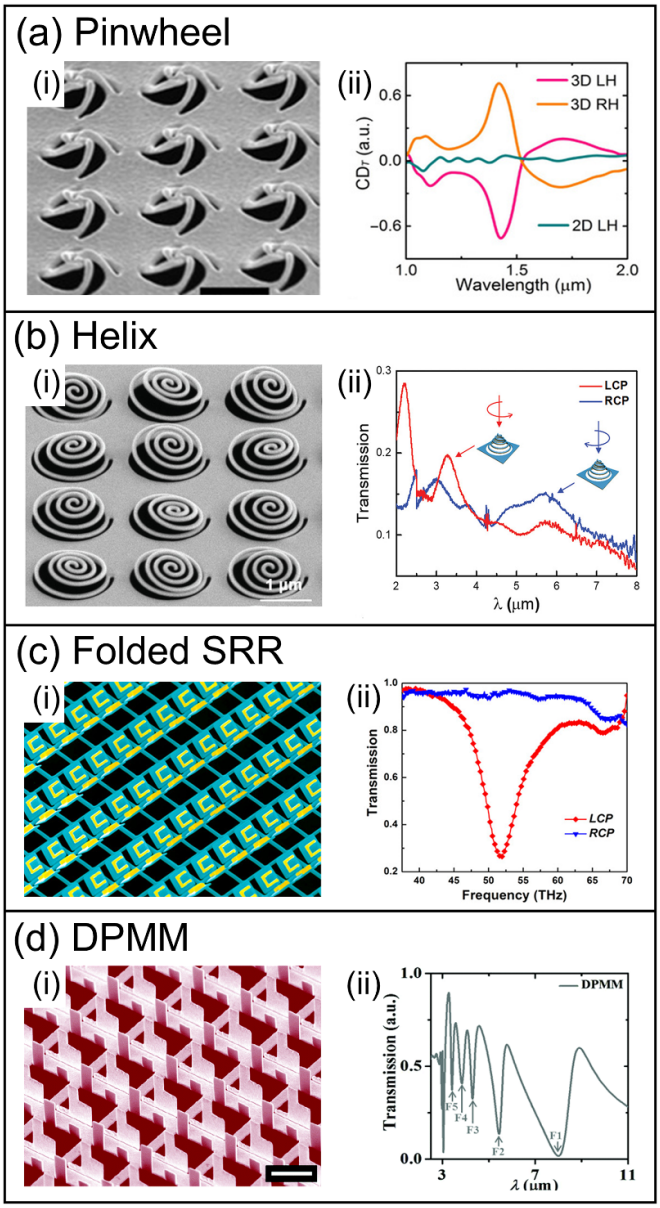

Figure 7. Optical chirality on nanomembrane origami/kirigami structures. (a) Nanomembrane kirigami with giant optical chirality [101]. Reproduced with permission from [101]. CC BY-NC 4.0. (i) SEM image and (ii) CD spectra of pinwheel array. (b) Helix array for enhanced broadband near-field optical chirality [161]. Reproduced with permission from [161]. CC BY-NC-ND 4.0. (i) SEM image and (ii) transmission spectra of helix array. (c) Spin-selective transmission in chiral folded metasurfaces Reprinted with permission from [28]. Copyright (2019) American Chemical Society. (i) Schematic and (ii) transmission spectra of folded SRR array [28]. (d) Five-fold plasmonic Fano resonances with giant bisignate circular dichroism [153]. Reproduced from [153] with permission from the Royal Society of Chemistry. (i) SEM image and (ii) transmission spectrum of DPMM array.

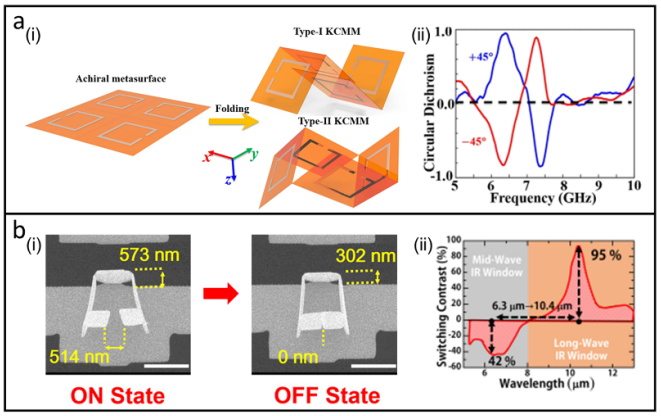

Figure 8. Optical reconfigurable nanomembrane origami/kirigami. (a) Reconfigurable nanomembrane origami for tunable chirality [213]. Reproduced from [213]. CC BY 4.0. (i) Schematic illustration of KCMMs. (ii) Corresponding measured CD spectra. (b) Tunable metasurface of SRR arrays for reversible optical change in infrared region [154]. Reprinted with permission from [154]. Copyright (2016) American Chemical Society. (i) Top-view SEM images of the rotation process from 'ON' to 'OFF'. (ii) Measured reflection spectra of the metasurface at different resonant states.

spin-selective transmission in the infrared region is observed in figure 7(c)-(ii). The intrinsic chirality is controllable by changing the folding angle of the metasurface relative to the base surface, which can also firmly support Fano resonance. Vertical folded SRRs are proposed to get Fano resonances with ultra-high refractive index sensitivity [183]. By changing the asymmetric arms of SRRs, this configuration with novel 3D plasma conduction coupling can induce different Fano resonances [212]. In addition, due to the special localized electric field distribution, Tian *et al* [153] proposed a folding chiral metasurface with double-plate-based metamaterials (DPMM) in figure 7(d)-(i). DPMMs array can support a five-fold plasmonic Fano resonance shown in figure 7(d)-(ii), as well as a significant bisignate CD effect with the magnitude of 0.8 by theoretical analysis. The 'bridge' in the double plate can be applied as a flipped ruler to manipulate optical chirality, including the handedness selectivity and the switching of CD signal.

Nanomembrane origami/kirigami assembly can result in vertical displacements through actuating the deformable unit, thus offering an ideal technique for reconfigurable photonics [151, 213]. With optical reconfiguration, various optical properties can be tuned by the deformation of origami/kirigami. Jing *et al* [213] reported a reconfigurable chiral metasurface nanomembrane folded by kirigami to switch the handedness. Two different 3D folded metamaterial nanomembranes are made from the same 2D precursor as shown in figure 8(a)-(i). By stretching the designed SRRs array, the toroidal resonances can be switched between nonchiral and chiral states. Figure 8(a)-(ii) shows the noticeable change of CD effects with different folding angles of zero and others. By controlling the direction of deformation, kirigami-based chiral metamaterials (KCMMs) of Miura-Ori SRRs array can also be applied to switch the high value of CD effect and chirality state [151]. More importantly, the relative density of origami nanomembrane can be decreased to only 2% of that of unfolded structure [151]. Based on nano SRRs array, Mao *et al* [154] manufactured a split-ring structure capable of tuning its optical properties. Figure 8(b)-(i) shows the gap of split-ring structures decreases from 514 nm to zero, while the state of the device switch from 'ON' to 'OFF', which induces a significant

change in the light–matter interaction. The arms of the folding structures contact each other by the deformation induced by Joule heat, which is revisable. By changing the gap width, the optical behavior could be tuned. As shown in figure 8(b)-(ii), reversible switch process induced by electrothermal change can be observed with a high switching contrast of 95% in the IR spectral region. In visible and near-infrared regions, broadband nonresonant and narrowband resonant optical reconfigurations are obtained on the nanomembrane kirigami [154].

The research on 3D complicated metastructures including pinwheels, spirals, and folding surfaces with strong chirality will help to understand and design novel optical micro/nano structures, with relatively simple 3D origami/kirigami fabrication strategies. The advanced applications of chiral optical system in optical communication, photon-spin selecting devices, ultrasensitive biosensing, polarization imaging, quantum information processing, and more could be expected in the future.

3.5. Complex optoelectronic devices/systems based on nanomembrane assembly

Traditional planar optoelectronic devices/systems can be converted into various 3D structures by assembling interconnected semiconductor devices and in some cases, by adopting the template method namely pick-place mentioned above [156, 214]. The pick-place approach that can generate complete optoelectronic system also gives birth to great application potential [134].

Photodetection systems based on 3D nanomembrane origami/kirigami are explored for more possibility. For example, 3D photodetection system was prepared on elastic substrates by utilizing compressive buckling. Figure 9(a)-(i) presents a 3D photodetection system made from Ti/SiO_2 nanomembrane by buckling assembly [156]. The system can support the modulation of optical sensing by changing the structures with sensor array on it. As shown in figure 9(a)-(ii), the photocurrent intensity can be tuned by changing the substrate strain, leading to weak (stage 1) and strong (stage 2) responses at the flat and 3D states, when a green laser is incident at a 45° angle on the photodetection system. Similar 3D hemispherical structures consisting of 2D material (i.e. graphene and MoS_2) nanomembranes can also be obtained via a similar approach for photodetection [49].

The 3D complex assembled structures can also be engaged in biomimetic optical components and image sensors for realization of various nature vision systems. In order to get close to eyes, an artificial eye sensor system consisting of many sensor blocks will be formed into hemisphere with the assistance of a template. The advantages of artificial eye system are high vision, large field of view, wavelength-free imaging, improved aberration correction and depth of field [215]. The low bending stiffness of nanomembranes allows high-performance photodetectors to curve with micrometer-scale radius [134], and compact hemispherical photodetector array by 3D assembly can easily be achieved [133]. Katiyar *et al* [162] reported a hemisphere eye sensor system containing Si nanomembrane photodetector arrays on polyimide (PI) film as shown in figure 9(b)-(i). The Si nanomembrane photodetector pixels were biaxially stretched through pneumatic pressure–induced bulging, which leads to a shrunk bandgap, enhance photoresponsivity and extend the Si absorption limit up to 1550 nm (figure 9(b)-(ii)).

Owing to the intrinsic properties of 2D materials, figure 9(c)-(i) presents an artificial eye sensor system consisting of array of high density sensors, which is designed based on the MoS_2-graphene heterostructure nanomembrane [55]. Due to the existence of MoS_2, this hemispherical curved image sensor system exhibits infrared radiation blindness and is capable to acquire pixelated optical signals. In figure 9(c)-(ii), the artificial eye sensor system with a high-density sensor array captures the letter sigma (Σ) in high resolution by integrating a single plano-convex lens. Hemispherical curved image-sensing arrays have potential in photodetection as soft implantable optoelectronic devices. The prepared miniaturized device is able to remove the metal wires connecting the pixels and also replaces the traditional complex actuators required to form the hemispheres [55, 133, 215]. Similar to the imaging sensor, Gao *et al* [164] reported a compliant skin-like photonic nanomembrane device, that combines thermochromic liquid crystal as colorimetric temperature indicators for the visualization of thermal measurements (figure 9(d)-(i)). Figure 9(d)-(ii) shows the steady state response of the device to changes in temperature between 32 °C and 39 °C. With proper calibration, the temperature extracted can be determined with a digital camera and computational tools for relating the results to underlying skin thermal processes [164].

Except for the normal photodetection, nanomembrane origami/kirigami can be endow with other functionalities for applications in e.g. biosensing [216]. Specifically, implantable devices serving temporary diagnosis or therapy, which need to provide intimate optical coupling to biological tissues for a finite time period, are expected to be fabricated by nanomembrane [217]. Bai *et al* [137] proposed flexible transient optical waveguides and surface-wave biosensors of monocrystalline Si nanomembrane. Due to the construction of filamentary structures from Si nanomembranes in figure 9(e)-(i), the high refractive index of silicon confine tight optical mode at sub-microscales, similar to the size of a single cell, which can precise delivery of light to targeted tissues [165]. Figure 9(e)-(ii) shows good consistency between the experimental and simulation results for the case of a U-shaped device in sensing ethanol, water and their mixtures, showing the potential in biosensing. On the other hand, implant nanomembrane devices are also used for brain research.

Gao *et al* [164] integrated III–V nanomembrane light emitting diode (LED) as a simulation source with electrochemical probe (figure 9(f)-(i)) for brain cell-specific modulation. LED determines the behavior of neurons, while the electrochemical probe can detect dopamine level [218]. Experimental results demonstrate that continuous blue stimulations suppress activities by hyperpolarization and photocurrents of neurons change accordingly.

These approaches to preparing biomimetic optoelectronic devices/systems possess the advantages of being relatively simple and low-cost, and the performance could be further

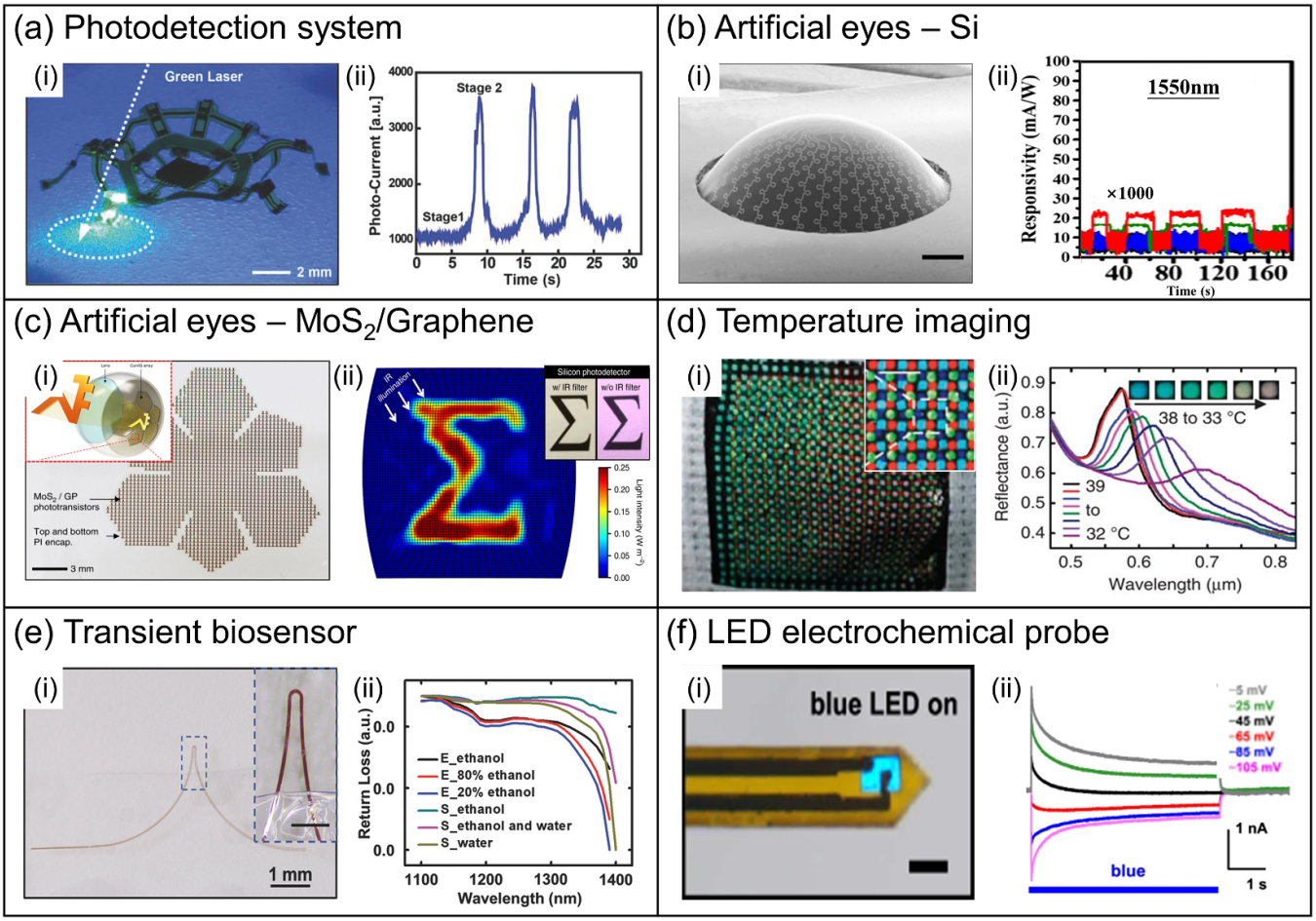

Figure 9. Complex optoelectronic devices/systems based on nanomembrane assembly. (a) Mechanically guided 3D assembly for photodetection [156]. [156] John Wiley & Sons. [Copyright © 2018 WILEY-VCH Verlag GmbH & Co. KGaA, Weinheim]. (i) Photograph of 3D buckled photodetector. (ii) Photocurrent under room lighting before 3D transformation (stage 1) and after transformation (stage 2). (b) Artificial eye sensor system from Si nanomembrane [162]. Reproduced with permission from [162]. CC BY-NC 4.0. (i) SEM image of convex hemispherical shape of PI film contains Si nanomembrane photodetector array. (ii) Strain-dependent transient photoresponse of device under incident lights of 980 and 1550 nm. (c) Artificial eye sensor system composed of MoS_2-graphene curved image sensor array [55]. Reproduced from [55]. CC BY 4.0. (i) Schematic of the shape and materials of the sensor array. (ii) Sigma-shaped image captured by the system. (d) Temperature imaging sensor [164]. Reproduced from [164], with permission from Springer Nature. (i) Photograph of the device with integrated patterns of dots that have fixed colors for calibration. (ii) Reflectance measured at a single pixel from 32 °C to 39 °C. (e) Transient Si nanomembrane waveguide-based biosensor [137]. [137] John Wiley & Sons. [Copyright © 2018 WILEY-VCH Verlag GmbH & Co. KGaA, Weinheim]. (i) Photograph of the sensor with U shape. (ii) Transmission spectrum of a U-shaped transient biosensor immersed in a mixture of water and ethanol, as measured in terms of the return loss. E presents experimental measurements, S presents simulation results. (f) III–V nanomembrane LED integrated with optoelectrochemical probe for optogenetic stimulation [165]. Reproduced from [165], with permission from Springer Nature. (i) Optical image of a micro-LED probe with blue emission. (ii) Measured photocurrents of neurons with potentials varied from −105 to −5 mV (bottom to top), under continuous blue light illumination.

enhanced with optimized design. The combination of device miniaturization and simplicity of design also lays a practical foundation for integration of these 3D structures with traditional electronic devices.

4. Summary and outlook

In this review, we summarize the recent progress of assembled nanomembranes-based 3D structures and their applications in the field of nanophotonics and optoelectronics (figure 10). As defined, the thickness of nanomembrane is between the atomic and macroscopic scales which makes them exhibit many unique properties that are quite different from the macroscopic counterpart. Due to the compatibility with traditional CMOS backplane systems, semiconductor nanomembrane including group IV and III–V materials were first introduced. In addition, inorganic materials such as pure metals, oxides and diamond-like materials can also be prepared in the form of nanomembranes. Nanomembranes can also be obtained from organic materials as well as 2D materials like graphene and MoS_2. The application of various materials brings diversity and possibilities to nanomembrane platforms.

With the development of micro/nano manufacturing, nanomembranes can be successfully prepared by bottom–up or top–down methods. Then, nanomembranes are released by combining a patterning process to create a pre-defined shape

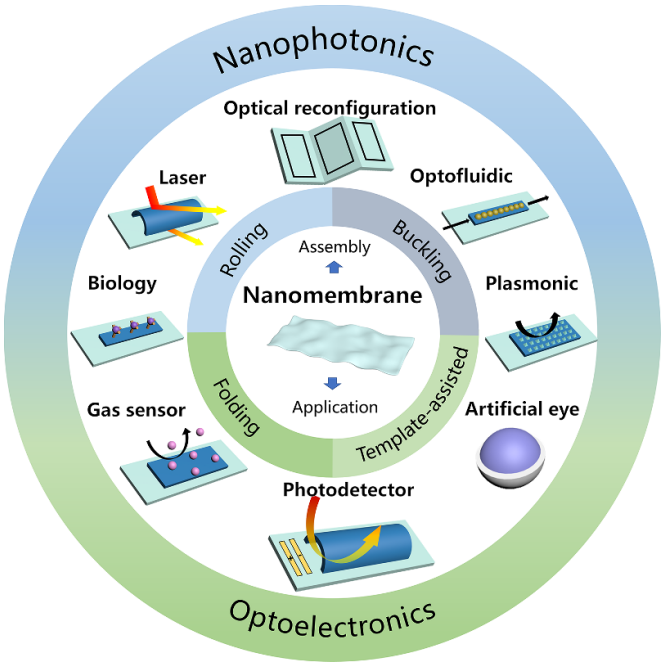

Figure 10. Summary of assembly methods and nanooptical/optoelectronic applications of nanomembranes.

with an etching process. Based on the multilayer nanomembrane, we summarize a series of fracturing technology and basic research of nanoscience, 2D to 3D nanomembrane assembly approaches, such as rolling, folding, bending and pick-place methods. Complex 3D micro/nano structures including microtubes, micro pinwheels, microcubes and folded metasurfaces can be constructed by the 3D assembly. These complicated 3D structures have unique geometric shapes and new properties that are different from flat nanomembranes.

Various applications of these micro/nano 3D nanomembrane devices in nanophotonics and optoelectronics have been reviewed. In order to control the light field, rolled-up microtube have been applied as optical microcavities due to their unique light confinement effect.

While 3D micro/nano structures based on origami/kirigami technology have been applied to study optical chirality and optical reconfiguration. In the field of optoelectronics, based on the unique rolled-up structure design and the corresponding light field regulation, the performance of the corresponding photodetector has been significantly improved. In addition to traditional photodetector systems, 3D complex structures built by nanomembrane assembly technology can also realize bionic optical elements and image sensors mimicking visual systems in nature.

While significant development has been made in nanooptics and optoelectronics applications of 3D nanomembrane assembly structures, there are still several significant gaps in fully overcoming the challenges encountered by Moore's Law. For example, although nanoscale 3D assembly can be prepared by the methods described above, nanochip applications with high integration density are rarely reported. In addition, the stability and the fineness ratio of preparing these 3D micro/nano structures need to be further improved in order to meet the mass requirements of industrial production. As for practical 3D structure devices, plenty of research is still needed in the future to explore the structure-function relationship of 3D structures based on nanomembrane assembly. The certainty and controllability of fabrication and its influence on device performance also need further research efforts.

Data availability statement

No new data were created or analyzed in this study.

Acknowledgments

This work is supported by the National Key Technologies R&D Program of China (2021YFA0715302 and 2021YFE0191800), the National Natural Science Foundation of China (61975035 and 51961145108), the Science and Technology Commission of Shanghai Municipality (22ZR1405000 and 20501130700) and the Program of Shanghai Academic Research Leader (19XD1400600).

ORCID iDs

Gaoshan Huang https://orcid.org/0000-0002-0525-7177
Yongfeng Mei https://orcid.org/0000-0002-3314-6108

References

[1] Tang R, Li G and Li C 2020 *Opt. Express* **28** 5731–40
[2] Long M, Wang P and Fang H 2019 *Adv. Funct. Mater.* **29** 1803807
[3] Wang H P, Li S and Liu X 2021 *Adv. Mater.* **33** 2003309
[4] Miao J, Zhang F 2019 *Laser Photonics Rev.* **13** 1800204
[5] Zhang Y, Ma Y and Wang Y 2021 *Adv. Mater.* **33** 2006691
[6] Qiu Q and Huang Z 2021 *Adv. Mater.* **33** 2008126
[7] Liu H, Lei Y and Shen H 2019 *Opt. Commun.* **447** 24–29
[8] Zhang R, Shao D and Fu Z 2016 *IEEE J. Sel. Top. Quantum* **23** 1–7
[9] Wang B, Dong F and Li Q-T 2016 *Nano Lett.* **16** 5235–40
[10] Sedaghat S and Zarifkar A 2017 *Opt. Commun.* **382** 167–75
[11] Wang H, Zhen H and Li S 2016 *Sci. Adv.* **2** e1600027
[12] Chen C, Youngblood N and Peng R 2017 *Nano Lett.* **17** 985–91
[13] Zhou L Y, Fu J and He Y 2020 *Adv. Funct. Mater.* **30** 2000187
[14] Vyatskikh A, Delalande S and Kudo A 2018 *Nat. Commun.* **9** 1–8
[15] Wang X Q, Yang S Y and Tian Q S 2021 *Angew. Chem., Int. Ed. Engl.* **60** 5213–9
[16] Cho M, Yun J and Kwon D 2018 *ACS Appl. Mater. Interfaces* **10** 12870–7
[17] Zhou X F, Tian Z and Kim H J 2019 *Small* **15** 1902528
[18] Seo J H, Zhang K and Kim M 2016 *Adv. Opt. Mater.* **4** 120–5
[19] Sim K, Rao Z L and Zou Z N 2019 *Sci. Adv.* **5** aav9653
[20] Das T, Chen X and Jang H 2016 *Small* **12** 5720–7
[21] Chen C, Li C and Min S W 2021 *Nano Lett.* **21** 8385–92
[22] Csutak S M, Schaub J D and Wu W E 2002 *IEEE Photonics Technol. Lett.* **14** 516–8
[23] Pierre A, Deckman I and Lechene P B 2015 *Adv. Mater.* **27** 6411

[24] Yao Y, Liang Y Y and Shrotriya V 2007 *Adv. Mater.* **19** 3979
[25] Li L S, Huang Y Y and Peng J B 2014 *J. Mater. Chem.* C **2** 1372–5
[26] Yin Y, Pang J and Wang J 2019 *ACS Appl. Mater.* **11** 15891–7
[27] Yoo C, Ko T J and Han S S 2021 *Nanoscale Adv.* **3** 3028–34
[28] Yang S, Liu Z and Hu S 2019 *Nano Lett.* **19** 3432–9
[29] Chun I S, Challa A and Derickson B 2010 *Nano Lett.* **10** 3927–32
[30] Py C, Reverdy P and Doppler L 2007 *Phys. Rev. Lett.* **98** 156103
[31] Tian Z, Huang W and Xu B 2018 *Nano Lett.* **18** 3688–94
[32] Freund L B and Suresh S 2004 *Thin Film Materials: Stress, Defect Formation and Surface Evolution* (Cambridge: Cambridge University Press)
[33] Huang G S and Mei Y F 2012 *Adv. Mater.* **24** 2517–46
[34] Jakšić Z and Matovic J 2010 *Mater. Horiz.* **3** 165–200
[35] Tian Z, Zhang L and Fang Y F 2017 *Adv. Mater.* **29** 1604572
[36] Goykhman I, Desiatov B and Khurgin J 2012 *Opt. Express* **20** 28594–602
[37] Song E, Si W and Cao R 2014 *Nanotechnology* **25** 485201
[38] Feng P, Monch I and Harazim S 2009 *Nano Lett.* **9** 3453–9
[39] Hochbaum A I, Chen R K and Delgado R D 2008 *Nature* **451** 163
[40] Rogers J A 2014 *MRS Bull.* **39** 549–56
[41] Menard E, Lee K J and Khang D Y 2004 *Appl. Phys. Lett.* **84** 5398–400
[42] Kim M, Liu S C and Kim T J 2016 *Opt. Express* **24** 16894–903
[43] Um D S, Lee Y and Lim S 2016 *ACS Appl. Mater. Interfaces* **8** 26105–11
[44] Chuang S L 2012 *Physics of Photonic Devices* (New York: Wiley)
[45] Wang X, Cui X and Bhat A 2018 *Appl. Phys. Lett.* **113** 201105
[46] Marçal L A B, Rosa B L T and Safar G A 2014 *ACS Photonics* **1** 863–70
[47] Dastjerdi M, Djavid M and Arafin S 2013 *Semicond. Sci.* **28** 094007
[48] Xie C, Mak C and Tao X M 2017 *Adv. Funct. Mater.* **27** 1603886
[49] Lee W, Liu Y and Lee Y 2018 *Nat. Commun.* **9** 1417
[50] Kaushik S and Singh R 2021 *Adv. Opt. Mater.* **9** 2002214
[51] Yan F, Zhao L and Patane A 2017 *Nanotechnology* **28** 27LT01
[52] Mak K F, Lee C and Hone J 2010 *Phys. Rev. Lett.* **105** 136805
[53] Radisavljevic B, Radenovic A and Brivio J 2011 *Nat. Nanotechnol.* **6** 147–50
[54] Lopez-Sanchez O, Lembke D and Kayci M 2013 *Nat. Nanotechnol.* **8** 497–501
[55] Choi C, Choi M K and Liu S 2017 *Nat. Commun.* **8** 1–11
[56] Jaksic Z, Vukovic S M and Buha J 2011 *J. Nanophoton.* **5** 051818
[57] Maier S A 2007 *Plasmonics: Fundamentals and Applications* vol 1 (New York: Springer) p 245
[58] Lee S, Kang K and Choi H 2021 *Appl. Sci.* **11** 6562
[59] Chen Y, Ouyang Z and Gu M 2013 *Adv. Mater.* **25** 80–85
[60] An J R, Zhao X Y and Zhang Y N 2022 *Adv. Funct. Mater.* **32** 2110119
[61] Huang W, Zhou J C and Froeter P J 2018 *Nat. Electron.* **1** 305–13
[62] Novoselov K S, Geim A K and Morozov S V 2004 *Sci. Adv.* **306** 666–9
[63] Zhang L, Liang J and Huang Y 2009 *Carbon* **47** 3365–8
[64] Ciesielski A and Samorì P 2014 *Chem. Soc. Rev.* **43** 381–98
[65] Song E M, Guo Q L and Huang G S 2017 *ACS Appl. Mater. Interfaces* **9** 12171–5
[66] Kay E 1971 *Ann. Rev. Mater. Sci.* **1** 289–312
[67] Montes L, Román J M and García-Casas X 2021 *Adv. Mater. Interfaces* **8** 2100767
[68] Yang Z, Surrente A and Tutuncuoglu G 2017 *Nano Lett.* **17** 2979–84
[69] Huang G, BolañOs QuiñOnes V A and Ding F 2010 *ACS Nano* **4** 3123–30
[70] Xu C, Pan R and Guo Q 2019 *Adv. Opt. Mater.* **7** 1900823
[71] Li M, Liu D and Wei D 2016 *Adv. Sci.* **3** 1600003
[72] Kafizas A, Carmalt C J and Parkin I P 2013 *Coord. Chem. Rev.* **257** 2073–119
[73] Huang W, Wang X and Sheng M 2003 *Mater. Sci.* **98** 248–54
[74] Plesa C and Dekker C 2015 *Nanotechnology* **26** 084003
[75] Wang Y, Ying C and Zhou W 2018 *Sci. Rep.* **8** 1–9
[76] Ohering M 2002 *Materials Science of Thin Films, Deposition and Structure* (Elsevier)
[77] Johnson R W, Hultqvist A and Bent S F 2014 *Mater. Today* **17** 236–46
[78] Leskelä M and Ritala M 2002 *Thin Solid Films* **409** 138–46
[79] Huard C M, Zhang Y T and Sriraman S 2017 *J. Vac. Sci. Technol.* A **35** 031306
[80] Vendamme R, Onoue S-Y and Nakao A 2006 *Nat. Mater.* **5** 494–501
[81] Wang F and Wang X 2014 *Nanoscale* **6** 6398–414
[82] Park M, Do K and Kim J 2015 *Adv. Healthcare Mater.* **4** 992–7
[83] Chan E P and Lee S C 2017 *J. Polym. Sci.* B **55** 412–7
[84] Cheng W, Campolongo M J and Cha J J 2009 *Nat. Mater.* **8** 519–25
[85] Li D, Fan Y and Han G 2020 *ACS Appl. Mater.* **12** 10039–49
[86] Yin X, Li H and Han L 2021 *Small* **17** 2008056
[87] Huan J, Hu L F and Fang X S 2014 *ACS Appl. Mater. Interfaces* **6** 1462–9
[88] Kim B, Tripp S L and Wei A 2001 *J. Am. Chem. Soc.* **123** 7955–6
[89] Cai R, Yang D and Lin K T 2019 *J. Am. Chem. Soc.* **141** 1725–34
[90] Boles M A, Engel M and Talapin D V 2016 *Chem. Rev.* **116** 11220–89
[91] Boker A, He J and Emrick T 2007 *Soft Matter* **3** 1231
[92] Sanchez-Iglesias A, Grzelczak M and Altantzis T 2012 *ACS Nano* **6** 11059–65
[93] Shi S and Russell T P 2018 *Adv. Mater.* **30** 1800714
[94] Li Y M, Song Y and Jiang Y C 2017 *Adv. Funct. Mater.* **27** 1701066
[95] Redl F X, Cho K S and Murray C B 2003 *Nature* **423** 968–71
[96] Wang D Y, Duan H W and Mohwald H 2005 *Soft Matter* **1** 412–6
[97] Gong S, Zhao Y M and Yap L W 2016 *Adv. Electron. Mater.* **2** 1600121
[98] Huang G, Mei Y and Cavallo F 2009 *J. Appl. Phys.* **105** 016103
[99] Huang M, Cavallo F and Liu F 2011 *Nanoscale* **3** 96–120
[100] Shen Y, Zhou J and Liu T 2013 *Nat. Commun.* **4** 1–9
[101] Liu Z, Du H and Li J 2018 *Sci. Adv.* **4** eaat4436
[102] Park S H, Yuan G and Chen D 2014 *Nano Lett.* **14** 4293–8
[103] Spierings G 1993 *J. Mater. Sci.* **28** 6261–73
[104] Fernández S, De Abril O and Naranjo F 2011 *Sol. Energy Mater.* **95** 2281–6
[105] Mei Y F, Kiravittaya S and Benyoucef M 2007 *Nano Lett.* **7** 1676–9
[106] Li J-X, Lu B-R and Shen Z 2011 *Microelectron. Eng.* **88** 1792–4
[107] Xu J, Wood G S and Mastropaolo E 2021 *ACS Appl. Mater.* **13** 38792–8
[108] Fan X, Smith A D and Forsberg F 2020 *Microsyst. Nanoeng.* **6** 1–17
[109] Madejski G R, Briggs K and Desormeaux J P 2019 *Adv. Mater. Interfaces* **6** 1900684
[110] Huang W, Yang Z and Kraman M D 2020 *Sci. Adv.* **6** eaay4508

[111] Roberts M M, Klein L J and Savage D E 2006 *Nat. Mater.* **5** 388–93
[112] Carlson A, Bowen A M and Huang Y 2012 *Adv. Mater.* **24** 5284–318
[113] Meitl M A, Zhu Z-T and Kumar V 2006 *Nat. Mater.* **5** 33–38
[114] Xu X C, Subbaraman H and Hosseini A 2012 *Opt. Lett.* **37** 1020–2
[115] Yang H J, Zhao D Y and Chuwongin S 2012 *Nat. Photon.* **6** 615–20
[116] Cheng X and Zhang Y 2019 *Adv. Mater.* **31** 1901895
[117] Yang S, Wang Y and Kong Y 2022 *Adv. Opt. Mater.* **10** 2102158
[118] Mei Y, Thurmer D J and Deneke C 2009 *ACS Nano* **3** 1663–8
[119] Prinz V Y 2003 *Microelectron. Eng.* **69** 466–75
[120] Cavallo F, Songmuang R and Ulrich C 2007 *Appl. Phys. Lett.* **90** 193120
[121] Songmuang R, Rastelli A and Mendach S 2007 *Appl. Phys. Lett.* **90** 091905
[122] Hu J, Bando Y and Zhan J 2005 *Appl. Phys. Lett.* **87** 113107
[123] Tian Z, Xu B and Hsu B 2018 *Nano Lett.* **18** 3017–23
[124] Huang W, Koric S and Yu X 2014 *Nano Lett.* **14** 6293–7
[125] Bell D J, Dong L and Nelson B J 2006 *Nano Lett.* **6** 725
[126] Zhang L, Ruh E and Grützmacher D 2006 *Nano Lett.* **6** 1311–7
[127] Zong Y, Zhang X and Wu Y 2021 *Prog. Nat. Sci.* **31** 865–71
[128] Li M, Yang Q and Liu H 2016 *Small* **12** 4492–500
[129] Chen S, Chen J and Zhang X 2020 *Light Sci. Appl.* **9** 1–19
[130] Cui A, Liu Z and Li J 2015 *Light Sci. Appl.* **4** e308–e
[131] Xu S, Yan Z and Jang K-I 2015 *Science* **347** 154–9
[132] Choi W M, Song J and Khang D-Y 2007 *Nano Lett.* **7** 1655–63
[133] Zhang Y, Yan Z and Nan K 2015 *Proc. Natl Acad. Sci.* **112** 11757–64
[134] Yan Z, Zhang F and Liu F 2016 *Sci. Adv.* **2** e1601014
[135] Zhang K, Jung Y H and Mikael S 2017 *Nat. Commun.* **8** 1782
[136] Saada G, Layani M and Chernevousky A 2017 *Adv. Mater. Technol.* **2** 1600289
[137] Bai W B, Yang H J and Ma Y J 2018 *Adv. Mater.* **30** 1801584
[138] Kim J, Lee M and Shim H J 2014 *Nat. Commun.* **5** 1–11
[139] Yoon J, Lee S M and Kang D 2015 *Adv. Opt. Mater.* **3** 1313–35
[140] Wu Z L, Moshe M and Greener J 2013 *Nat. Commun.* **4** 1586
[141] Shyu T C, Damasceno P F and Dodd P M 2015 *Nat. Mater.* **14** 785
[142] Pelton M, Santori C and Vuckovic J 2002 *Phys. Rev. Lett.* **89** 233602
[143] Bekele D, Yu Y and Yvind K 2019 *Laser Photonics Rev.* **13** 1900054
[144] Sak M, Taghipour N and Delikanli S 2020 *Adv. Funct. Mater.* **30** 1907417
[145] Mccall S L, Levi A F J and Slusher R E 1992 *Appl. Phys. Lett.* **60** 289–91
[146] Kong Y, Zhao Z and Wang Y 2021 *ACS Appl. Mater.* **13** 58104–13
[147] Medina-Sa´Nchez M, Ibarlucea B and Pe˜Rez N S 2016 *Nano Lett.* **16** 4288–96
[148] Briche R, Benamrouche A and Cremillieu P 2020 *APL Photonics* **5** 106106
[149] Dastjerdi M, Djavid M and Mi Z 2015 *Appl. Phys. Lett.* **106** 021114
[150] Deng T, Zhang Z H and Liu Y X 2019 *Nano Lett.* **19** 1494–503
[151] Wang Z, Jing L and Yao K 2017 *Adv. Mater.* **29** 1700412
[152] Cho J H, Keung M D and Verellen N 2011 *Small* **7** 1943–8
[153] Tian X, Liu Z and Lin H 2018 *Nanoscale* **10** 16630–7
[154] Mao Y, Pan Y and Zhang W 2016 *Nano Lett.* **16** 7025–9
[155] Xu W, Li T and Qin Z 2019 *Nano Lett.* **19** 7941–9
[156] Kim B H, Liu F and Yu Y 2018 *Adv. Funct. Mater.* **28** 1803149
[157] Guo Q, Fang Y and Zhang M 2016 *IEEE Trans. Electron. Devices* **64** 1985–90
[158] Gao L, Zhang Y and Zhang H 2015 *ACS Nano* **9** 5968–75
[159] Xu L, Wang X and Kim Y 2016 *ACS Nano* **10** 6156–62
[160] Chen S S, Liu Z G and Du H F 2021 *Nat. Commun.* **12** 1299
[161] Tseng M L, Lin Z H and Kuo H Y 2019 *Adv. Opt. Mater.* **7** 1900617
[162] Katiyar A K, Thai K Y and Yun W S 2020 *Sci. Adv.* **6** eabb0576
[163] Yuan H C and Ma Z Q 2006 *Appl. Phys. Lett.* **89** 212105
[164] Gao L, Zhang Y H and Malyarchuk V 2014 *Nat. Commun.* **5** 4938
[165] Li L, Lu L and Ren Y 2022 *Nat. Commun.* **13** 1–14
[166] Jia P P, Zuber K and Guo Q Q 2019 *Mater. Horiz.* **6** 1005–12
[167] Vahala K J 2003 *Nature* **424** 839–46
[168] Cao H and Wiersig J 2015 *Rev. Mod. Phys.* **87** 61–111
[169] Pollinger M, O'shea D and Warken F 2009 *Phys. Rev. Lett.* **103** 053901
[170] Wang J, Zhan T R and Huang G S 2014 *Laser Photonics Rev.* **8** 521–47
[171] Li Y, Feng L and Su X 2017 *Opt. Express* **25** 18072–80
[172] Tian Z, Li S and Kiravittaya S 2018 *Nano Lett.* **18** 8035–40
[173] Ma L B, Li S L and Fomin V M 2016 *Nat. Commun.* **7** 10983
[174] Lan Y W, Li S L and Cai Z Y 2017 *Opt. Commun.* **386** 72–76
[175] Mei Y, Huang G and Solovev A A 2008 *Adv. Mater.* **20** 4085–90
[176] Chen Y P, Yin Y and Ma L B 2021 *Adv. Opt. Mater.* **9** 2100143
[177] Wang J, Yin Y and Yang Y-D 2019 *ACS Photonics* **6** 2537–44
[178] Huang G S, Kiravittaya S and Quinones V A B 2009 *Appl. Phys. Lett.* **94** 141901
[179] Li X L 2011 *Adv. Opt. Photonics* **3** 366–87
[180] Bottner S, Li S L and Jorgensen M R 2014 *Appl. Phys. Lett.* **105** 121106
[181] Kipp T, Welsch H and Strelow C 2006 *Phys. Rev. Lett.* **96** 077403
[182] Strelow C, Rehberg H and Schultz C M 2008 *Phys. Rev. Lett.* **101** 127403
[183] Wang J, Zhan T R and Huang G S 2012 *Opt. Express* **20** 18555–67
[184] Fang Y, Li S and Mei Y 2016 *Phys. Rev.* A **94** 033804
[185] Quinones V A B, Ma L B and Li S L 2012 *Opt. Lett.* **37** 4284–6
[186] Yin Y, Li S and Engemaier V 2016 *Phys. Rev.* A **94** 013832
[187] Yin Y, Li S and Böttner S 2016 *Phys. Rev. Lett.* **116** 253904
[188] Briukhanova D, Habib M and Issah I 2021 *Appl. Phys. Lett.* **119** 141101
[189] Wang X Y, Yin Y and Dong H Y 2021 *ACS Nano* **15** 20694
[190] Wang X, Yin Y and Dong H 2021 *ACS Nano* **15** 18411–8
[191] Miao S D, Chen D C and Madani A 2015 *Adv. Opt. Mater.* **3** 187–93
[192] Lin X Y, Fang Y F and Zhu L J 2016 *Adv. Opt. Mater.* **4** 936–42
[193] Zhang J, Zhong J and Fang Y 2014 *Nanoscale* **6** 13646–50
[194] Pelton M, Vuckovic J and Solomon G S 2002 *IEEE J. Quantum Electron.* **38** 170–7
[195] Li F and Mi Z 2009 *Opt. Express* **17** 19933–9
[196] Yin Y, Li S and Giudicatti S 2015 *Phys. Rev.* B **92** 241403
[197] Yin Y, Chen Y and Saei Ghareh Naz E 2017 *ACS Photonics* **4** 736–40
[198] Gao L 2017 *Small* **13** 1603994
[199] Kim J H, Ko T-J and Okogbue E 2019 *Sci. Rep.* **9** 1–10
[200] Ko T J, Wang M J and Yoo C 2020 *J. Phys. D: Appl. Phys.* **53** 313002
[201] Yoo C, Kaium M G and Hurtado L 2020 *ACS Appl. Mater. Interfaces* **12** 25200–10
[202] Zhang P P, Nordberg E P and Park B N 2006 *New J. Phys.* **8** 200

[203] Cavallo F, Songmuang R and Schmidt O G 2008 *Appl. Phys. Lett.* **93** 143113
[204] Zhang F, Huang G and Mei Y 2021 *J. Electron. Mater.* **50** 3111–5
[205] Gansel J K, Thiel M and Rill M S 2009 *Science* **325** 1513–5
[206] Mun J, Kim M and Yang Y 2020 *Light Sci. Appl.* **9** 1–18
[207] Rodrigues S P, Lan S and Kang L 2017 *Nat. Commun.* **8** 1–8
[208] Wang Z, Cheng F and Winsor T 2016 *Nanotechnology* **27** 412001
[209] Zhang S, Park Y-S and Li J 2009 *Phys. Rev. Lett.* **102** 023901
[210] Liu Z, Du H and Li Z-Y 2018 *APL Photonics* **3** 100803
[211] Arora W J, Smith H I and Barbastathis G 2007 *Microelectron. Eng.* **84** 1454
[212] Liu Z G, Li J F and Liu Z 2017 *Sci. Rep.* **7** 8010
[213] Jing L, Wang Z and Zheng B 2018 *NPG Asia Mater.* **10** 888–98
[214] Leong W, Abdullah M Z and Khor C 2012 *Microelectron. Reliab.* **52** 744–56
[215] Lee G J, Choi C and Kim D H 2018 *Adv. Funct. Mater.* **28** 1705202
[216] Wang H C, Sun P C and Yin L 2020 *Infomat* **2** 527–52
[217] Han M, Wang H and Yang Y 2019 *Nat. Electron.* **2** 26–35
[218] Liu C, Zhao Y and Cai X 2020 *Microsyst. Nanoeng.* **6** 1–12